Roles of keratin filaments on β-cell mitochondrial behavior and functionality

Anup Shrestha

Turun yliopisto
University of Turku

Master's thesis

Faculty of Medicine, University of Turku

Department of Biosciences/Cell Biology, Åbo Akademi University

01.05.2019

Master's degree of Biomedical Imaging

Credits: 45 ECTS

Supervisors:

1. Diana Toivola (Associate Professor)
2. Jonas Silvander (PhD)

Examiners:

1. ……...
2. …..……

Passed:

Grade:

UNIVERSITY OF TURKU

Faculty of Medicine

ANUP SHRESTHA: Role of keratin filaments on β-cell mitochondrial behavior and functionality

Master's thesis, 72 pp

Specialization level: Light microscopy imaging

May 2019

Abstract

Keratin (K) intermediate filaments (IFs) are IFs of epithelial cell, and one of the most abundant IFs found in the cells, Keratins have various functions including stress protection, cell signaling and protein targeting. In pancreatic β-cells K8 and K18 are the main keratins expressed. Presence or absence of keratin IFs have shown to change the mitochondrial morphology in pancreatic β-cells which in turn likely influences the insulin production in the β-cells. Reduction in insulin production or insulin resistance causes diabetes mellitus (DM). Type I and type II DM was responsible for 1.6 million deaths according to study by World Health Organization (WHO) in 2016. The aim of this thesis work was to find the role of keratin IFs in mitochondrial morphology and dynamics to better understand the insulin production by using a cancerous pancreatic cell line, Murine Insulinoma 6 (MIN6) cells. Various microscopes were used to acquire images from the fluorescently labelled fixed and live cell samples followed by image analysis. In this study, it was found that the overexpression of wild type K8/K18 significantly decreased the mitochondrial motility and insulin vesicle count per unit area of the cell while mitochondrial count per unit cell area, mitochondrial fragmentation level and cell area were significantly increased. Likewise, the K18R90C mutation which disrupts keratins filaments, decreased the cell area, insulin vesicle count per unit cell area and mitochondrial count per unit cell area. The liver disease associated mutation K8G62 resulted in higher mitochondrial fragmentation and higher insulin vesicle count per unit area compared to the K8WT/K18WT overexpressing MIN6 cells. In conclusion, these results provide valuable insight to understand the role of keratin in the mitochondrial behavior and functionality which influence the insulin production in the pancreatic cells.

KEYWORDS: Keratin – Mitochondria – Insulin – MIN6 cells - β-cells – diabetes – Insulin vesicles – TOM complex – Islets of Langerhans

List of Abbreviations

ΔΨm	Mitochondrial membrane potential
AIP	Arylhydrocarbon receptor-interacting protein
ATP	Adenose triphosphate
DM	Diabetes mellitus
EBS	Epidermolysis bullosa simplex
EH	Epidermolytic hyperkeratosis
EPPK	Epidermolytic palmoplantar keratoderma
ER	Endoplasmic reticulum
FAD	Flavin adenine dinucleotides
IBD	Inflammatory bowel disease
IF	Intermediate filament
ISC	Ionic sulfur clusters
K	Keratin (similarly K8 for Kreatin 8)
$K8^{-/-}$	Keratin 8 knock out
$K8^{+/+}$	Keratin 8 wild type
MCD	Meesmann's corneal dystrophy
MF	Microfilament
MFN	Mitofusin
MIN6	Murine insulinoma 6
MT	Microtubule
mtDNA	Mitochondrial Deoxyribonucleic acid
MW	Molecular weight

NAD	Nicodinamideadenine dinucleotides
OPA1	Optic atrophy type 1
OXPHOS	Oxidative phosphorylation
R	Arginine
RER	Rough endoplasmic reticulum
TCHP	Trichoplein
TEM	Transmission electron microscope
TIM	Translocase of inner membrane
TOM	Translocase of outer membrane

CONTENTS

1 LITERATURE REVIEW

1.1 The Pancreas

1.1.1 Structure, tissue and cell types of the pancreas

The human pancreas is an elongated glandular organ located in the abdominal cavity. The pancreas sits on the curvature of the duodenum behind the stomach (figure 1). Anatomically, the pancreas is divided into 3 regions or lobes: head, body and tail (Braganza, 1994). The head of the pancreas, the widest region of the pancreas, lies at the curvature of the duodenum and the body tapers to the left side and ends near the spleen which is called the tail of the pancreas (Dolenšek et al., 2015). All pancreatic regions consist of adipose, connective and lymphatic tissues. Each lobe is subdivided into smaller lobules where each major glandular lobule receives one major duct. The primary lobule is composed of acinar cells, whose main function is to produce digestive enzymes that are secreted into pancreatic duct and eventually joins to common bile duct (Reichert and Rustgi, 2011). The proximal part of pancreatic ducts is lined with simple squamous epithelium while the distal part is lined with simple cuboidal epithelium (Henry et al., 2019). Similarly, there are spherical shaped clusters of cells known as Islet of Langerhans that produce blood glucose regulating hormones which are poured directly to the bloodstream (Dubois, 1999; Henry et al., 2019).

1.1.1.1 Islets of Langerhans

A small portion of the total pancreatic volume comprises of islets of Langerhans (1-4%) which have endocrinal functions (Saito et al., 1978; Dolenšek et al., 2015) (figure 1). These islets were first discovered by Paul Langerhans in 1869 where he saw oval cellular aggregates of β-cells which was found to produce a hormone called insulin by Frederick G. Banting and his team in 1922 (Kulkarni, 2004). These islets consist of several types of endocrine cells, which can be few to thousands in number. There are four major endocrine cells found in the islets of Langerhans including α-cells that produce glucagon, β-cells that produce insulin, δ-cells producing somatostatin and γ-cells producing pancreatic polypeptide (Bertelli and Bendayan, 2005; Reichert and Rustgi, 2011).

β-cells are the most abundant endocrine cells in endocrine pancreas comprising 50-70% of the total cells in islets while the α-cells comprises 20-40% and δ/γ-cells comprise less than

10% of the total cell population of the islets (Rahier et al., 1981; Cabrera et al., 2006; Kim et al., 2009).

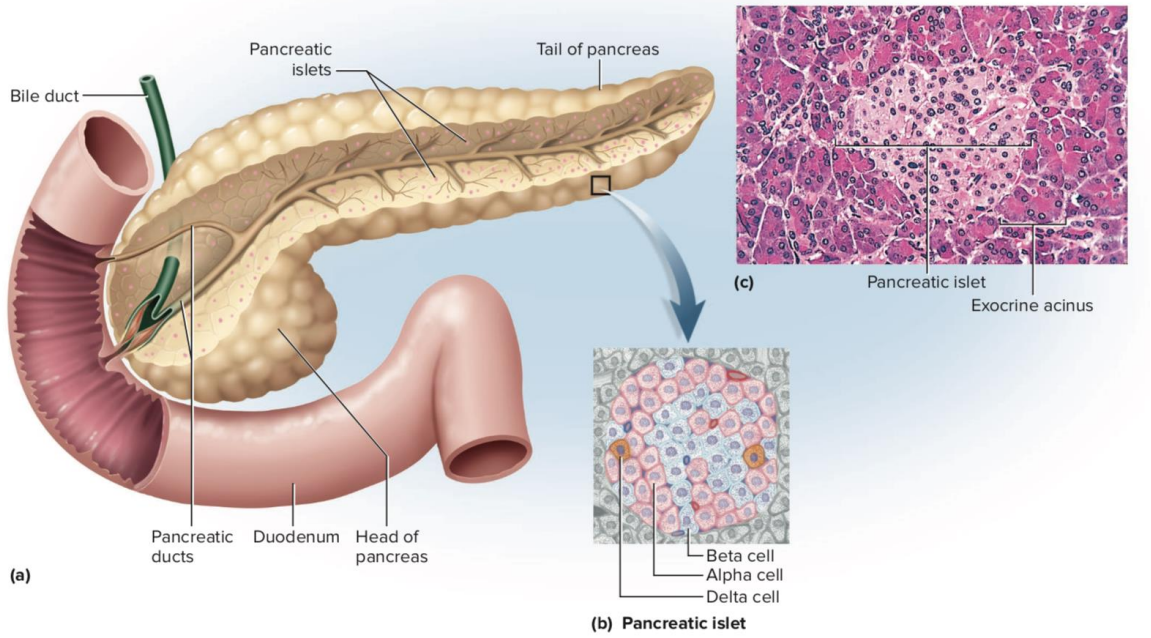

Figure 1. The pancreas. (a) The pancreas is located at the curvature of the duodenum. Exocrine pancreatic secretions merge with bile duct and pour into duodenum. (b) Cells of a pancreatic islet. (c) Hematoxylin and eosin staining of pancreatic tissue taken by a light microscope. It shows the light colored pancreatic islets surrounded by darker stained pancreatic acini (Saladin, 2018).

1.1.1.2 β-cells

β-cells are the most important cells in the islet of Langerhans as they produce the insulin hormone responsible for blood glucose homeostasis. These cells are very sensitive to the nutrients which trigger the production of insulin to the bloodstream (Kulkarni, 2004). β-cells has electron dense insulin granules in their cytoplasm shown by the electron microscope in figure 2 (Alam et al., 2013). These granules are the storage units for insulin and release the insulin in short burst when blood glucose level increment is detected (Michael et al., 2006).

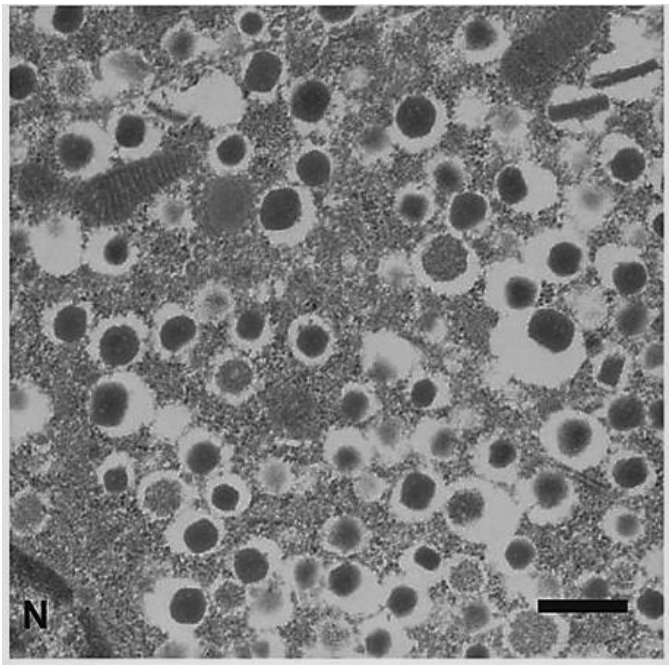

Figure 2. A β-cell with numerous insulin vesicles. Insulin cores appear darker due to high electron density. When blood glucose level elevates, these insulin vesicles are released from the β-cell by exocytosis. N represents the nucleus. Scale bar: 500nm (Alam et al., 2013).

1.1.2 Functions

The pancreas has two main functions: digestion of food by production of digestive enzymes, such as lipases, proteases and amylases, and glucose homeostasis by secretion of the hormones insulin and glucagon (Danielsson et al., 2014).

1.1.2.1 Exocrine functions

The exocrine part of the pancreas consists of acinar cells. The acinar cells are highly developed and secrete digestive enzymes (proteolytic, amylolytic, lipolytic and nuclease digestive enzymes) and transport them via the pancreatic ducts and duodenum (Whitcomb and Lowe, 2007; Pandol, 2010).

1.1.2.2 Endocrine functions

The most important function of the endocrine pancreas is to maintain blood glucose levels in the body. Glucose plays a highly significant role in a large number of metabolic pathways. It is also an essential nutritional requirement for the neurons. Glucose homeostasis in human blood stream is essential for proper wellbeing. The cells in pancreatic islets of Langerhans are responsible for the regulation of glucose levels in the body. The pancreatic α- and β- cells produce the hormones glucagon and insulin

respectively. Insulin promotes synthesis and storage of glycogen in liver and muscles and triglyceride by conversion of glucose to fatty acids in adipose tissues (Nussey and Whitehead, 2001). Glucagon, on the other hand, has counter regulatory functions of the insulin. It primarily acts on the liver, where it stimulates production of cAMP and through several cascades of intracellular events, glycogen is broken down to glucose and likewise production of glucose from amino acids (gluconeogenesis) (Nussey and Whitehead, 2001).

1.1.3 Major endocrine pancreatic diseases

Diabetes mellitus (DM) is the major disease related to the endocrine pancreas. The main symptom of DM is the elevated blood glucose concentration due to reduction of insulin production or/and insulin resistance (Nussey and Whitehead, 2001). There are two types of DM, Type I DM and Type II DM. Both types of diabetes cause hyperglycemia but the pathophysiology and etiology are different. In type I DM, the β-cells are depleted progressively due to autoimmune response of the body. Hence the patients are dependent on the exogenous insulin (Chiang et al., 2014). Type II DM is mainly characterized by the insulin resistance and accounts for 90-95% of the total diabetic patients. Type II DM does not cause destruction of β-cells (Nussey and Whitehead, 2001).

1.2 Insulin

1.2.1 Molecular structure of insulin and insulin vesicles

Insulin is a 51-residue anabolic peptide hormone containing two chains, A (21-residue) and B (30-redidue), connected by disulphide bonds forming a heterodimer. Insulin is produced by the β-cells of pancreatic islets when stimuli like elevation of blood glucose from food digestion is detected (Weiss et al., 2000). There are nearly 13,000 insulin granules ina single murine β-cell (about 10% of the total volume of a cell) (Dean, 1973; Fu et al., 2013). The molecular structure of insulin can be present in hexamer form (stable and found in stored form) or in a monomer form, which is highly reactive due to the small size (Dunn, 2005). Insulin vesicles are composed of cargo ions, small molecules and proteins in two different compartments: the condensed core and acidic outer solution (Michael et al., 2006). Pancreatic β-cells secrete about 70 insulin vesicles in a short burst with alternating intervals of 15-45 seconds (Michael et al., 2007).

1.2.2 Insulin production and regulation

The primary structure of insulin was discovered by Sanger in mid 1950's. It contained two-chain heterodimer, 21-residue-A-chain and 30-residue-B-chain connected to each other by two disulfide bonds (Weiss et al., 2000). Later on, in late 1960's, it was found that the precursor of the insulin molecule was proinsulin (9 kDa) which consists of a C domain joining the A- and B-chains. Proinsulin is broken down to insulin molecule and a free C-peptide by the action of trypsin–like enzymes. Likewise, a bigger precursor of proinsulin was discovered, called preproinsulin (12 kDa) (Chan et al., 1976; Weiss et al., 2000). The structure of preproinsulin includes proinsulin with additional 24-residue signal peptide of hydrophobic residues at the amino-terminus of the proinsulin (Weiss et al., 2000).

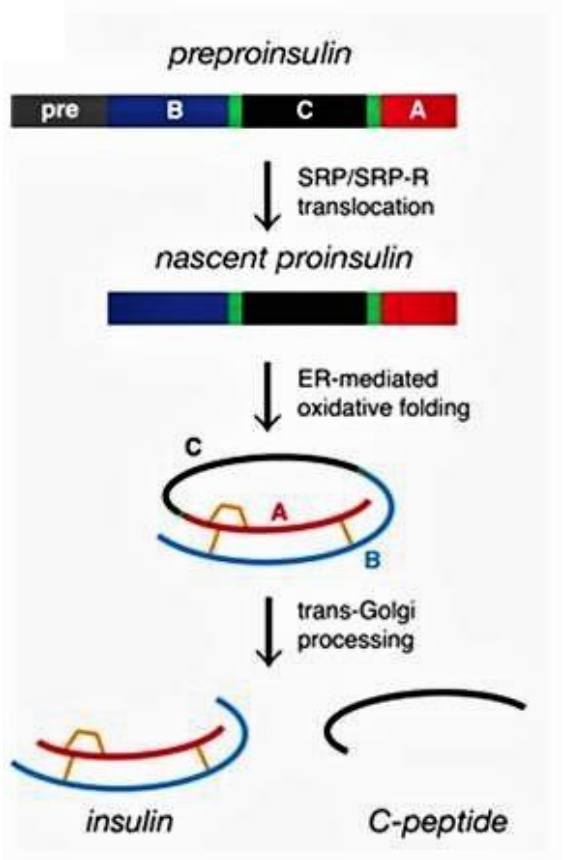

Figure 3. Biosynthesis and secretion of insulin molecule in pancreatic β-cells. The formation of insulin molecule begins with the formation of preproinsulin. The gray segment represents the signal peptide while the blue, red and black segments represent B-domain, A-domain and C-domain respectively. The green segments between B-C and C-A segments are the dibasic junctions. The unfolded preproinsulin produce proinsulin by the specific disulfide pairings in the rough endoplasmic reticulum (RER). Later on, the B-C and C-A junctions (green) are cleaved by the prohormone convertase and carboxypeptidase E to form mature insulin and free C-peptide in the golgi apparatus (Weiss, 2009).

Insulin is produced from the insulin gene by the formation of insulin mRNA. This mRNA produces preproinsulin and is eventually processed to insulin molecule. The mRNA encodes preproinsulin that is translated in rough endoplasmic reticulum (RER) and cleaved to proinsulin. Then the proinsulin undergoes rapid folding along with the formation of disulphide bonds to form a direct precursor of insulin which is still a proinsulin at this point (Patzelt et al., 1978; Weiss et al., 2000). This proinsulin is transported to the Golgi apparatus, where it is packaged into secretory granules and converted to native insulin, along with free C-peptide (figure 3) (Nishi et al., 1990; Weiss, 2009; Weiss et al., 2000).

Glucose stimulates the β-cells in pancreas to produce insulin. Glucose also helps in the activation of insulin gene transcription, stabilizes the insulin mRNA and translation (Welsh et al., 1985; Weiss et al., 2000; Poitout et al., 2006).

The amount of insulin release by the pancreatic β-cells is essential because abnormal fluctuation in glucose levels in blood can be life threatening and hence, it is strictly controlled by a series of stimulatory and inhibitory factors (Coore and Randle, 1964; Henquin, 2009). When the blood glucose level rises, β-cell metabolism increases, resulting in increase of ATP. It causes closing of the ATP-sensitive potassium (K^+) channel which decrease the flow of K^+ in the β-cells which in turn leads to membrane depolarization and influx of calcium ions (Ca^{++}) due to opening of Ca^{++} channel. This Ca^{++} influx promote the exocytosis of insulin vesicles (Gauthier and Wollheim, 2008; Henquin, 2009; Lang, 1999).

1.3 Cytoskeleton

Cytoskeleton of a cell is a complex mesh of fibrous elements consisting of microtubules (MTs), microfilaments (MFs) and intermediate filaments (IFs) (figure 4) (Lodish et al., 2000a), which are spread throughout the cytoplasm and/or the nucleus of the cell. Among these three cytoskeletal component, MFs have the smallest diameter of about 7 nm; microtubules have the largest diameter of about 23 nm while IFs lies in between with a diameter of approximately 10 nm. The fibrous structure of these cytoskeletal components is composed of smaller subunits. Actin is the major component in microfilaments while microtubules are comprised of tubulin. Intermediate filaments comprise a wide array of proteins such as keratins (K), vimentin and others outlined in section 1.3.1 (Herrmann et al., 2009; Wickstead and Gull, 2011). All three cytoskeletal components have their own various major roles in the cell. For instance, IFs give mechanical strength and resist

environmental stress, microtubules help in intracellular transport and locomotion while microfilaments determines the shape of the cell's surface and also helps in cell locomotion (Alberts et al., 2002a).

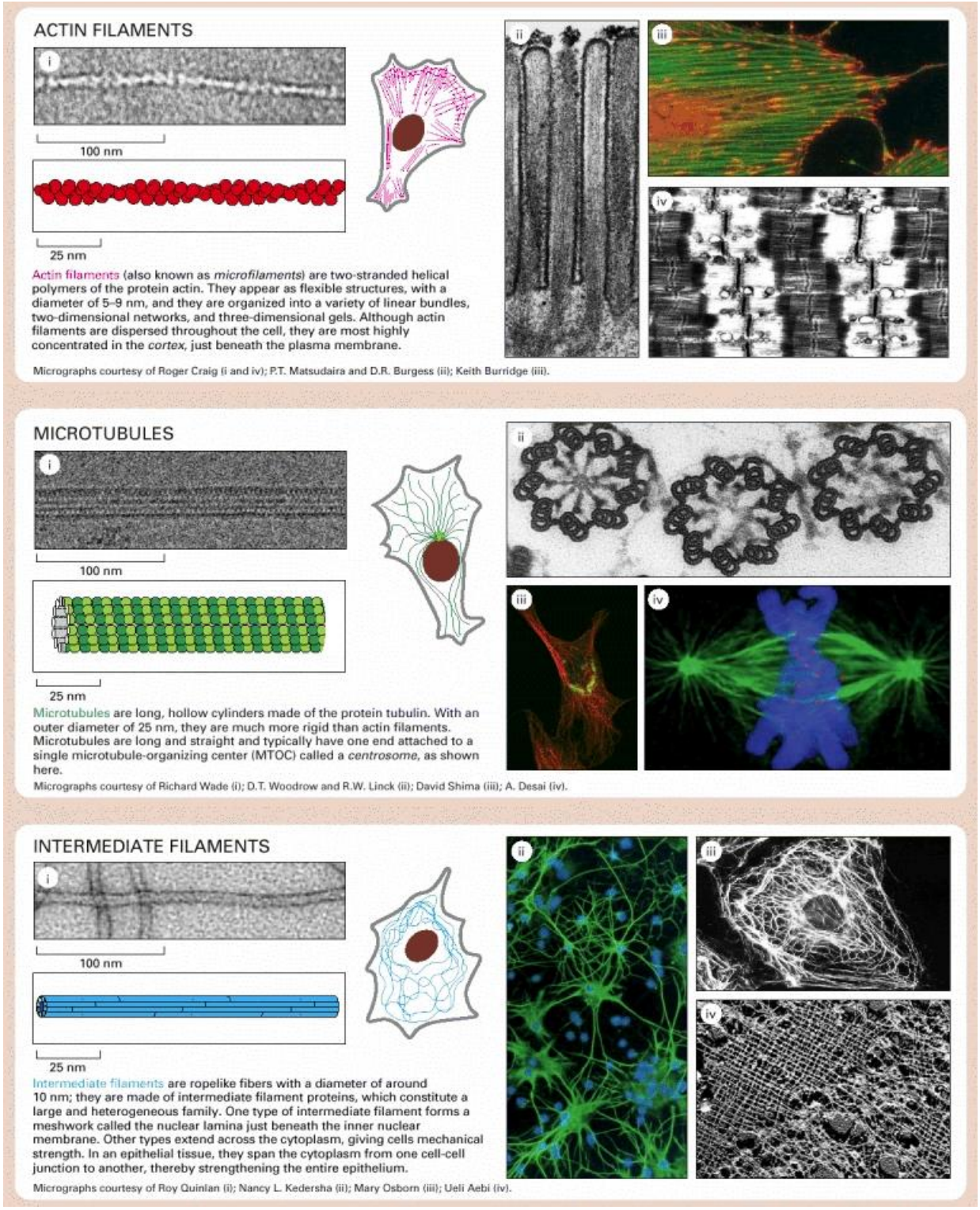

Figure 4. Components of cytoskeleton. Actin, microtubules and intermediate filaments are the three major types of cytoskeletal system with various functions and roles in a cell (Alberts et al., 2002a).

1.3.1 Intermediate filaments (IFs)

IFs are the commonly found cytoskeletal components in the cytoplasm of the cell. There are more than 50 types of IFs divided into six major groups according to the properties of their constituent amino acid groups: Acidic keratin filaments (Type I), basic keratin filaments (Type II), vimentin and desmin family (Type III), neurofilaments (Type IV), nuclear lamins (Type V) and nestin (Type VI) (Lodish et al., 2000b; Block et al., 2015). In humans, IFs are made up of insoluble proteins from more the 70 genes (Hesse et al., 2001). These proteins have a central α-helical rod domain and are flanked by different non-helical N- and C- terminals (Robert et al., 2016). These proteins form homopolymers or heteropolymers in different types of IFs. Hence, each cell type has its own unique IF type which modifies and adapts to the different mechanical properties of the cells in different tissues and stages of their development (Robert et al., 2016).

1.3.1.1 Functions of IFs

Generally, the main function of IFs is to give mechanical support for plasma membrane and reinforce the cells. IFs do not help the cells in mobility unlike the microfilaments and microtubules (Lodish et al., 2000b). IFs have various functions like regulation of apoptosis, cell growth, cell differentiation, signal transduction and migration (Schwarz and Leube, 2016). Similarly, they tend to organize the cytoplasmic space, influence the shape of nucleus, positioning of Golgi apparatus, mitochondria, lysosomes, centrosomes, ribosomes, melanosomes and junction between the cells and extracellular matrix (Mayerson and Brumbaugh, 1981; Sarria et al., 1994; Bauer and Traub, 1995; Chang et al., 2009; Guo and Zheng, 2015).

1.3.2 Keratins

Keratin filaments are the most abundantly found IFs and they build the IFs of all epithelial cells (about 80% of the total protein content in differentiated cells of stratified epithelia) (Moll et al., 1982; Steinert, 2001; Pekny and Lane, 2007). Keratins can resist the action of digestive enzymes like pepsin, trypsin and other dilute acids, alkali, water and organic solvents (Block, 1951; Steinert et al., 1982; Bragulla and Homberger, 2009). Keratins are insoluble in water but soluble in protein denaturing solutions like urea (Steinert et al.,

1982). The molecular weight (MW) of keratin proteins are found to be in the range of 40-70 kDa and the filament structure is about 10nm in diameter (T Sun et al., 1983).

1.3.2.1 Types of keratins

The keratin family is subdivided into two sub-families: type I (acidic) and type II (basic). This division is based on the isoelectric point (pI) where type I keratins have a pI of around 4.9-5.4 and type II keratins have pI of 5.5-6.5 (Moll et al., 1982; Bowden et al., 1984). Approximately 30% of the amino acids and sequences are similar in acidic and basic keratin types (Hanukoglu and Fuchs, 1983a). K1-K8, K71-K80 and K81-K86 belong to the type II or basic keratin sub family while K9-K23 and K25-K28 are included in type I or the acidic keratin sub family (Coulombe et al., 1989; Langbein et al., 1999; Coulombe and Omary, 2002; Schweizer et al., 2006). Type I and Type II keratin are obligate heteropolymers and form heterodimer structures (Moll et al., 2008).

K8 (MW=52.5 kDa, pI =6.1) is the primary keratin found in simple epithelia and along with K18, they are the first keratins to be synthesized in embryos (Moll et al., 1982; Pekny and Lane, 2007). K8 forms heterodimers, mainly with K18 or with K19 (Dale et al., 1985). K18 (MW= 44 kDa, pI = 5.5 in human) is expressed in most of the simple epithelia of urogenital tract, hepatocytes, bile ducts, renal tubules, intestines, bronchi and alveoli (Debus et al., 1982; Achtstätter et al., 1985; Hutton et al., 1998). K8 and K18 are the primary keratins in exocrine and endocrine pancreas while small amounts of K7 and K19 are also found in the exocrine pancreas (Ku et al., 1999). Likewise, K5 and its heterodimer partner K14 are the primary keratins of basal cells in the stratified epidermis (Pekny and Lane, 2007). K19, with MW of 40 kDa is the smallest keratin due to short tail domain, can partner up with K8, K5 or K7 (Eckert, 1988; Fradette et al., 1998). Similarly, each keratin type has its unique cell specificity and physiochemical properties (Bragulla and Homberger, 2009).

1.3.2.2 Structure of keratin filament

The amino acid chains in different keratins varies in number, sequence, polarity, charge and size but all types of keratin consist of a central α-helical rod domain, N-terminal head domain and C-terminal tail domain (Steinert et al., 1984; Coulombe et al., 2004; Bragulla and Homberger, 2009) (figure 5). Each of the head, tail and central domains are further divided into sub domains. These domains and subdomains help in different functions like

assembly of keratins and binding to signaling molecules and cell adhesion complexes (Steinert et al., 1984; Hatzfeld and Burba, 1994).

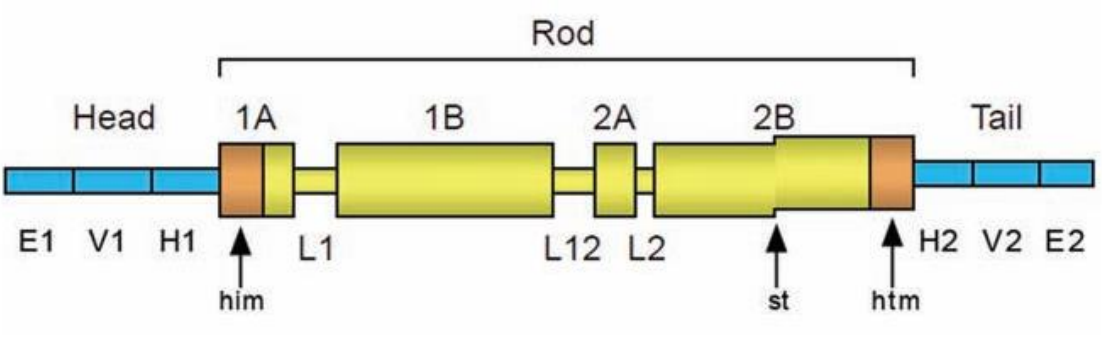

Figure 5. Structure of keratin molecule with domains and subdomains. A keratin protein molecule consists of a head, rod body and a tail. The rod comprises of subdomains linked by linker regions while the head and tail parts consists of amino acids capable of interacting with other biomolecules (Bragulla and Homberger, 2009).

The head domain (with N-terminus) may contain 50-100 positively charged amino acids that can interact with other molecules (Kazerounian et al., 2002; Herrmann and Aebi, 2004). The rod domain has about 310 amino acids with four α- helical sub domains, 1A, 1B, 2A and 2B, separated by linker regions, L1, L12 and L2 (Hanukoglu and Fuchs, 1983b; Coulombe and Omary, 2002; Herrmann and Aebi, 2004; Bragulla and Homberger, 2009). The α-helical component comprises of 38-45% of the whole keratin structure (Steinert, 1975) and consists of seven amino acids forming heptads which are necessary for the formation of the α- helix and coiled heterodimer (Eckert, 1988). The linker regions of the rod domain have a variable number of amino acid sequence and length. Alteration in the amino acid sequence, due to a mutation or a genetic disease that forms the rod domains, leads to the disruption in the formation of the coiled-coil structure of keratin filament. Heterodimers and tetramers so formed are damaged or fragmented (Smith et al., 2004). These mutations and abnormalities of keratin structure are observed in many diseases like epidermolysis bullosa simplex (EBS), pachyonychia congenital, cryptogenic liver cirrhosis, pancreatitis, cancer of colon, lungs and ovary (Cavestro et al., 2003; Hernandez et al., 2005; Moll et al., 2008; Omary et al., 2009; Wilson et al., 2014).

The tail domain (with C-terminus) is globular and non-helical structure (Er Rafik et al., 2004; Bragulla and Homberger, 2009). The rod domain and tail domain of partner keratins determines the diameter of the keratin filament. The tail domain also stabilizes the keratin filaments *in vitro* (Herrmann et al., 2000; Bousquet et al., 2001; Coulombe and Omary, 2002). Interactions of these domains and sub domains with adjacent keratin molecules result in the formation of heterodimers, tetramers and eventually mature keratin filaments (Wilson et al., 1992; Bragulla and Homberger, 2009).

The heterodimer structure is the building block of keratin filaments and it is formed by a equimolar amount of acidic and basic keratins from the rod domains in parallel orientation (Moll et al., 1982; Eichner et al., 1986; Er Rafik et al., 2004). Combination of heterodimers results in formation of tetramers which are mostly formed at the periphery of the cell. These tetramers act like the stored building blocks that can form keratin filaments when needed. (Bragulla and Homberger, 2009; Coulombe et al., 1998).

The secondary structure of keratin can be changed with the influence of mechanical forces like compression, tension, shearing due to stretching, internal osmotic pressures in cells or chemical processes (changes in pH, osmolarity, ionic strength, etc.) (Wilson et al., 1992; Bragulla and Homberger, 2009).

1.3.2.3 Major functions of keratins

The major function of keratin filaments is to provide mechanical support to the epithelial cells against stress. They also maintain structural integrity along with the mechanical resilience of the cellular structure (Coulombe and Omary, 2002) . Likewise, keratin filaments have direct or indirect roles in vital cellular processes like cellular osmolarity (Toivola et al., 2004), apoptosis (Gilbert et al., 2004) and regulation of protein synthesis (Kim et al., 2006).

1.3.2.4 Keratin mutations and related diseases

There are about 54 functional keratin genes in humans and among them, 21 has been linked with various hereditary disorders (Szeverenyi et al., 2008; Chamcheu et al., 2011). Abnormal levels of expression of these genes and mutations in coding sequences of these genes are known to cause or predispose various diseases (Toivola et al., 2015) . For example, mutation in K5 (nucleotide deletion, 1649delG) (Gu and Coulombe, 2005) or K14

(Arg125-Cys) (Ma et al., 2001) causes skin to lose the elastic property, being susceptible to breakage shear stress (stretching), causing epidermolysis bullosa simplex (EBS). Mutations in any one of the five keratin genes KRT6A, KRT6B, KRT6C, KRT16 or KLRT17 causes a rare autosomal disease known as pachyonychia congenital (Wilson et al., 2014). Corneal epithelia cells have K3 and K12 whose mutations cause an autosomal dominant disorder called Meesmann's corneal dystrophy (MCD), where the anterior corneal epithelium becomes very fragile, forming cysts and eventually rupture (Irvine et al., 1997). Likewise, K8 and K18 mutations are linked with several chronic and acute liver diseases like cryptogenic liver cirrhosis (Ku et al., 1995; Omary et al., 2009; Strnad et al., 2010) pancreatitis (Cavestro et al., 2003) and are possibly predisposing to inflammatory bowel disease (IBD) (Owens et al., 2004).

The keratin knockout ($K8^{-/-}$) mice models can develop several complications. For instance, $K8^{-/-}$ mice develop a TH2-type colitis (Habtezion et al., 2005) along with several other colonic abnormalities in ion transport, mistargeting of proteins, hyperplasia and diarrhea (Baribault et al., 1994). Likewise, $K8^{-/-}$ mice develop hemorrhage in liver and cause death in embryonic stage in C57BL/6 mice (Baribault et al., 1993). In another study, it was found that $K8^{+/-}$ mice were more sensitive to streptozotocin treatment and severe type I diabetes was developed compared to $K8^{+/+}$ mice (Alam et al., 2018).

Keratins also serve as markers for diagnosis of cancer. Epithelial tumors or adenocarcinomas in glandular tissues normally express K8, K18 and K19 but have abnormal levels of K7 and K20 according to the origin of the tissue or organ (Karantza, 2011). For example, K7 and K20 expression indicates advanced colorectal cancer (Hernandez et al., 2005), while uniform level of K7 along with variable level of K20 is associated with pancreatic, biliary tract, esophageal and gastric adenocarcinomas (Hernandez et al., 2005). Likewise $K7^{+}/K20^{-}$ phenotype is known to be found in ovarian, endometrial and lung adenocarcinomas (Moll et al., 2008) along with malignant salivary gland carcinomas (Nikitakis et al., 2004).

1.3.2.5 K18 R90C mutation

At the beginning and the end of the rod domain of all keratins, there are highly conserved areas where mutations are found in several skin diseases. The mutation near to the head domain has a highly conserved arginine (R), and is responsible for about 40% of all the

mutations found in EBS, epidermolytic hyperkeratosis (EH) and epidermolytic palmoplantar keratoderma (EPPK) in K14, K10 and K9 respectively (Ku et al., 1995). K18 along with its major partner K8 are the primary keratins in liver and endocrine pancreas. It is found that the transgenic mice which expresses genetically mutated K18 (K18 R90C) have disruptive keratin filaments (figure 6b) (Omary et al., 2002). The disruption is more severe in organs like pancreas and liver where K8/K18 are the major keratin types, and less severe in colon, where K8/K19 are the major keratins (Ku et al., 1995). Hence, certain points in the IFs, like R90 in K18 for the keratin IFs, plays a vital role in the assembly and in the formation of the IFs like keratins, vimentin, lamins, desmin, nestin and peripherin (Ku et al., 1995). This mutation has not been reported in human K18, probably due to its embryolethal properties (Omary et al., 2002; Porter and Lane, 2003).

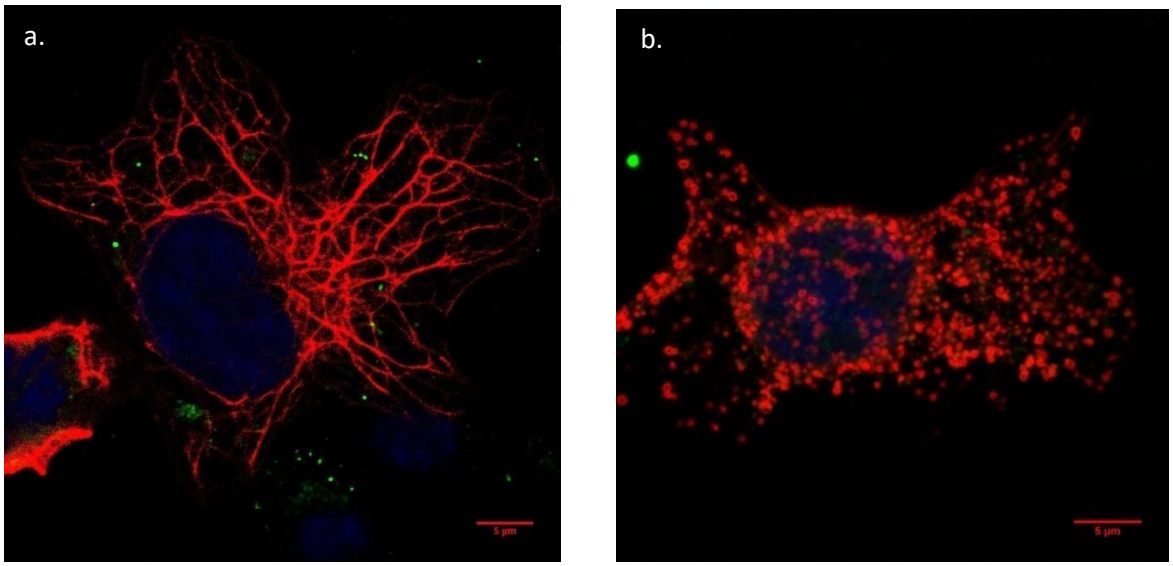

Figure 6. MIN6 cells showing, keratin (red), mitochondrial TOM20 (green) and nuclei (blue). (a) Normal keratin structure in murine insulinoma 6 (MIN6) cells overexpressing wild type K8 and K18 is shown where the structure of the keratin protein is long and undisrupted filament structures. (b) Keratin structure is disrupted due to the R90C mutation of K18 (lower). Scale bar = 5µm.

1.3.2.6 K8G62C mutation

K8 Glycine (G) 62 is also a highly conserved site and has a deep association with cirrhosis and liver fibrosis (Ku et al., 2005; Strnad et al., 2006). Transgenic mice overexpressing G62C are more prone to liver injury and apoptosis. The mutation also inhibits the nearby K8 phosphorylation site at Serine 74 (S74) (Ku and Omary, 2006).

1.4 Mitochondria

Mitochondria are rod shaped cell organelles which are spread throughout the cell cytoplasm. The major function of mitochondria is production of energy by the process of cell respiration, and subsequent production of energy in the form of adenosine triphosphate (ATP) due to the oxidation reactions of various molecules like glucose, lipids and proteins in the cells (Bonora et al., 2012; Shaw and Nunnari, 2002). Hence, mitochondria are also called 'the power house of the cell'. Likewise, the mitochondria are also involved in the synthesis of biomolecules, maintenance of calcium homeostasis, production of reactive oxygen species (ROS) and apoptosis (Held and Houtkooper, 2015). The number of mitochondria in a cell largely depends on the cell type, location and functionality of the cells. For example, liver and muscle cells have a maximum number of mitochondria, around 2000 (one fifth of total cell volume), since they require high amounts of energy, whereas red blood cells completely lack mitochondria as they travel passively in blood through the vascular pressures (Robin and Wong, 1988; Cole, 2016).

1.4.1 Structure of mitochondria

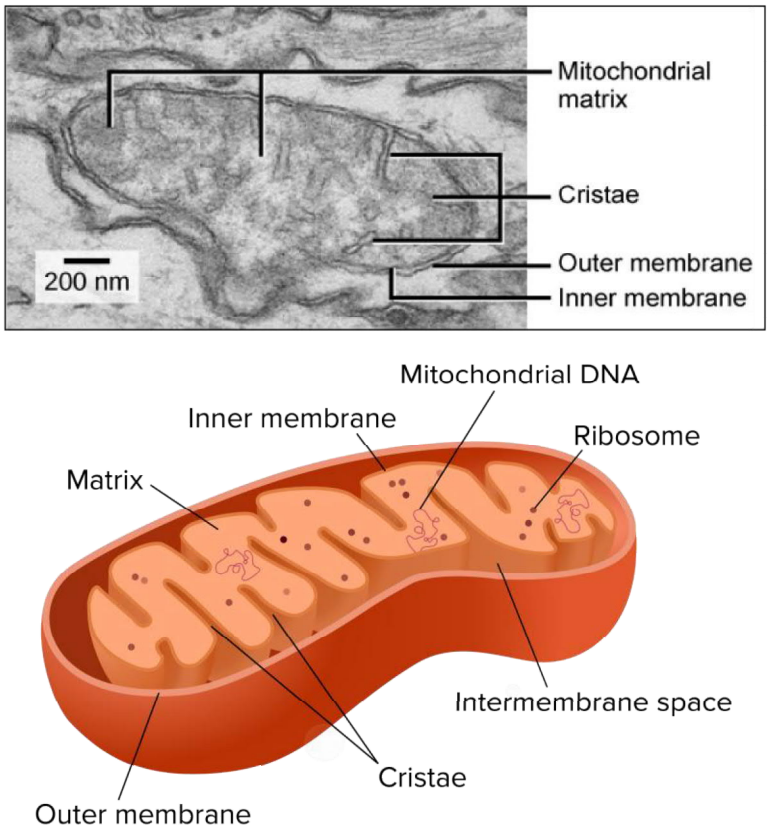

Figure 7. The electron microscope image of a mitochondrion (upper image) and 3D sketch of the mitochondrion (lower image). The mitochondria have a double membrane structure where the inner membrane is highly folded to form cristae that significantly increase the surface area for production ATP energy. Mitochondria also has its own DNA called mtDNA. (Retreived from http://www.khanacademy.org)

The basic shape of a mitochondrion is an elongated cylinder shape (figure 7) with an approximate diameter of 0.5-1 μ m, large enough to be seen through a light microscope and it is constantly changing through fission and fusion among themselves (Alberts et al., 2002b). There are two membranes in the mitochondrion structure, the outer membrane and a highly folded inner membrane. The folds of the inner membrane create an intermembraneous space between the two membranes, while the enveloped core consist of the mitochondrial matrix. Both membranes are composed of a phospholipid bilayer. The inner membrane of the mitochondria forms many folds known as cristae, which enclose the

central matrix. The matrix consist of the mitochondrial genetic materials and metabolic enzymes necessary for the oxidative metabolism of glucose and fatty acids to produce energy (Cooper, 2000). These folded structures provide a greater surface area for oxidative reactions. Similarly, in the inner membrane a large number of proteins involved in the oxidative phosphorylation and the molecular transport in and out of the mitochondria can be found. The inner membrane is the principal site of ATP generation. It is less permeable compared to the outer membrane and allows very selective molecules through porous units known as translocase of inner membrane (TIM) (Alberts et al., 2002b; Chacinska et al., 2009). The outer membrane allows large molecules (up to 6 kDa) to pass and is more permeable than the inner membrane. They also have aqueous porous structures known as translocase of outer membrane (TOM). The proteins called porins form channels within the outer membrane, which allow free diffusion of the molecules to and from the cytosol (Cooper, 2000; Alberts et al., 2002b).

1.4.2 Mitochondrial Membrane potential (ΔΨm) and ATP synthesis

Advanced eukaryotic cells need mitochondria for the efficient utilization of glucose to produce ATP. Without mitochondria, glycolysis alone produces 2 ATP molecules during conversion of glucose to pyruvate while by the help of mitochondria, a total of 30 molecules of ATP are generated which is about 90% more efficient than the process of glycolysis alone (Alberts et al., 2002b). After the glycolysis, the fatty acids and pyruvate are transported to the matrix through the inner membrane and converted to acetyl CoA by the oxidation of fatty acids. It is then followed by citric acid cycle where the acetyl group is converted or oxidized in the matrix and carbon atoms are released as waste CO_2 (Alberts et al., 2002b). This process activates the carrier molecules, reduced nicodinamide adenine dinucleotides (NADH) and fully oxidated flavin adenine dinucleotide (FADH2), which help in electron transport from the mitochondrial matrix to intermembraneous space entering the electron-chain transport (ECT) process. During ECT, NADH and FADH2 lose electrons to form NAD+ and FAD which is utilized in oxidative metabolism (figure 8) (Alberts et al., 2002b; Chacinska et al., 2009).

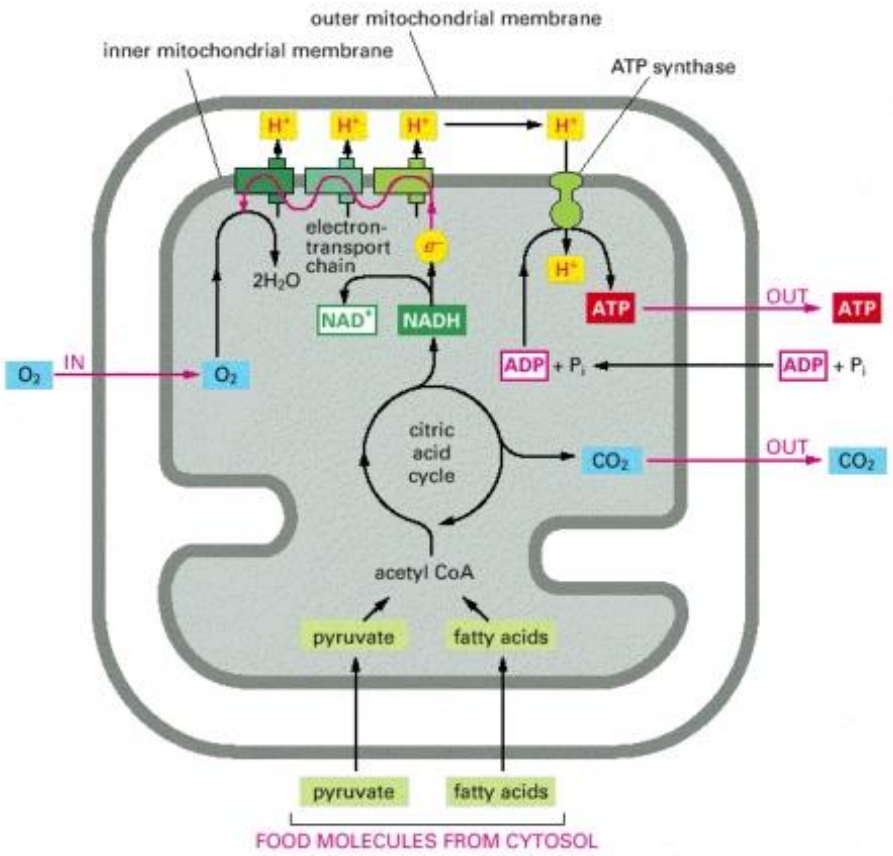

Figure 8. Generation of energy in the form of ATP in mitochondria. Acetyl CoA breaks down pyruvates and fatty acids and produce NADH in the matrix of the mitochondria. NADH is converted to ATP by going through electron transport chain in the inner membrane of the mitochondria (Alberts et al., 2002b).

Mitochondrial membrane potential helps in the generation of ATP and iron sulfur clusters (ISCs). ISCs help proteins in the mitochondria, cytosol and nucleus for performing essential functions like respiration, protein translation and genome maintenance in mitochondria (Veatch et al., 2009; Martínez-Reyes et al., 2016).

1.4.3 Translocase of outer membrane

TOM complex (figure 9) is the general gateway to all the mitochondrial preprotiens. These mitochondrial preproteins are the protein precursors carrying signal sequences that help in transportation of the mitochondrial proteins, synthesized in cytosol, in and out of the mitochondrial matrix (Pfanner et al., 1997). TOM complex comprises of TOM20, TOM22, TOM70 and TOM40, where TOM40 is a channel protein but TOM20, TOM22 and TOM70 are receptor proteins (Hoogenraad et al., 2002). TOM40 is a barrel shaped membrane-embedded central component protein which forms the protein importing pore with the

combination of TOM5, TOM6 and TOM7 (Hill et al., 1998; Verschoor and Lithgow, 1999; Becker et al., 2005).

TOM20 along with TOM70 are the major receptors in the TOM complex. They are anchored to the N-terminal transmembrane segment in the outer membrane and expose the hydrophilic domain to the cytosol receiving N-terminal presequences (Neupert and Herrmann, 2007). TOM20 along with the help of arylhydrocarbon receptor-interacting protein (AIP), help in import of the mitochondrial preproteins (Yano et al., 2003).

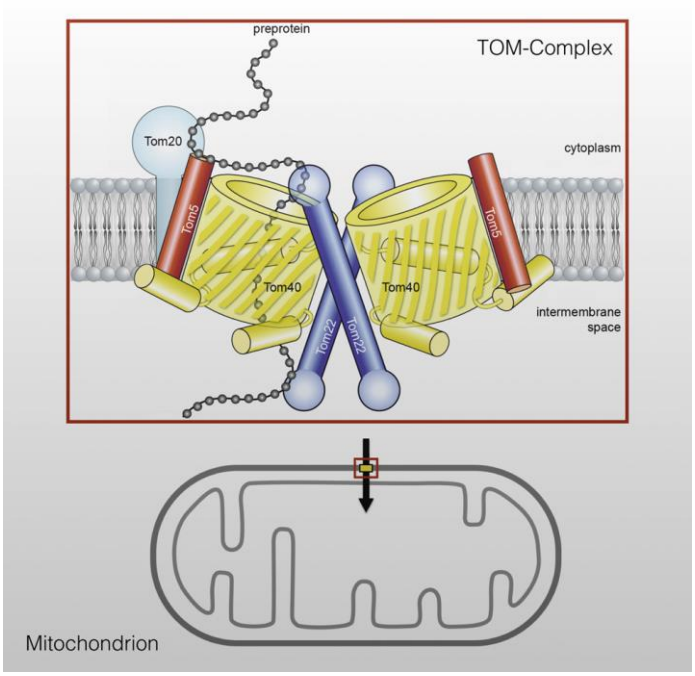

Figure 9. Translocase of outer membrane of mitochondria (TOM) complex. TOM complex comprises of various subunits which collectively helps in transportation of proteins from the cytosol to mitochondria. TOM20 lies at the outermost subunit of TOM complex (Bausewein et al., 2017).

1.5 Keratin and mitochondria

In a eukaryotic cells, generally IFs like keratin, vimentin, lamins, nestin and others are present. Apart from lamins, which are located in the nuclei, IFs are distributed throughout the cytoplasm (Herrmann et al., 2009; Schwarz and Leube, 2016). These IFs are involved in making the 3D scaffold for the cells and other novel functions. Since they act as an organizer of the cytoplasmic space, they interact with the cell organelles like mitochondria, Golgi bodies, lysosomes, ribosomes, lipid droplets and cellular junctions (Bauer and Traub, 1995; Kumemura et al., 2004; Silvander et al., 2017; Styers et al., 2004; Toivola et al.,

2005). More than 80 human related diseases are caused by alteration in the interaction of these organelles with the mutated IFs (Omary, 2009; Schwarz and Leube, 2016).There are several ways by which IFs like keratin can interact with mitochondria like binding, signaling and confinement of the mitochondria by the IFs (figure 10).

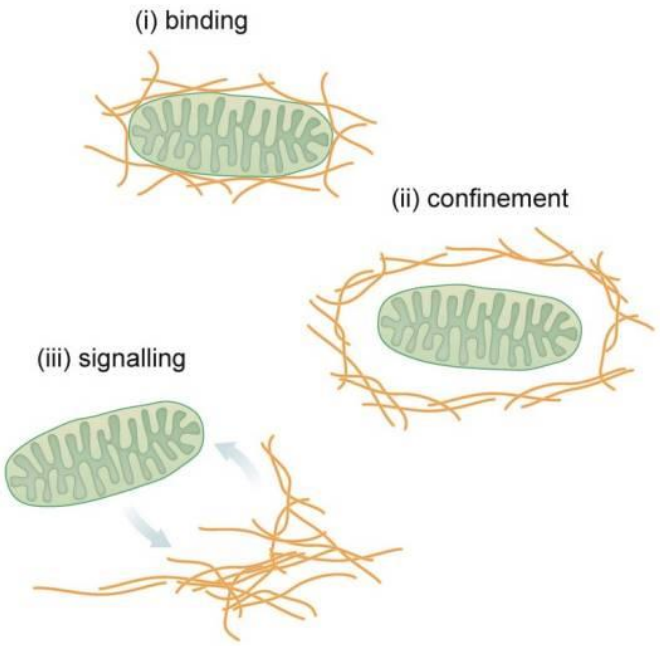

Figure 10. Hypothesis for interaction of IFs with mitochondria. It is hypothesized that IFs could interact with mitochondria in three major ways: (i) IFs can bind with mitochondria through molecular linkage (ii) IF can confine the mitochondria forming a network surrounding the mitochondria (iii) cell signaling between the IFs and mitochondria (Schwarz and Leube, 2016).

In pancreatic β-cells, loss of K8 cause abnormalities in mitochondrial structure where the mitochondria are smaller, more fragmented and round in structure with diffused cristae. The ΔΨm is lower in $K8^{-/-}$ β-cells and results in lower ATP production and subsequently lowers level of insulin secretion. Similarly, mitochondrial motility increases in $K8^{-/-}$ β-cells compared to $K8^{+/+}$ β-cells suggesting that keratin IF gives anchorage sites to the mitochondria in the cytoplasm (Silvander et al., 2017). Similarly, in liver cells absence or mutation of K8 and K18 results in changes in hepatocytic mitochondrial proteins, morphologically smaller and rounder mitochondria, decrease in ATP production and lower level of cytochrome C. Mice liver without K8 was more prone to injury and apoptosis as well (Kumemura et al., 2008; Tao et al., 2009). Hence, it is clear that the role of keratin in the morphology and function of mitochondria is crucial and needs to be further studied.

2 HYPOTHESES

K8 and K18 are the major keratins found in pancreatic β-cells and they have important roles in mitochondrial functionality and insulin production (Alam et al., 2013; Silvander et al., 2017). In $K8^{-/-}$ β-cells, K18 fails to form keratin filaments in the absence of a type II keratin partner which results in lower fasting blood glucose levels, higher glucose tolerance levels and higher insulin sensitivity (Alam et al., 2013). Insulinoma MIN6 cells that were used in this thesis study, closely resemble the pancreatic β-cells. However, WT ($K8^{+/+}$) and mutant variant of K8 and K18 were overexpressed since the MIN6 cells lacks these proteins. Nonetheless, they were excellent tools in this study and therefore used to test out the following hypotheses:

1. Higher levels of keratin in MIN6 cells increase the ΔΨm.
2. Mitochondria partially colocalize with keratin filaments at mitochondrial outer membrane in MIN6 cells overexpressing K8WT/K18WT and K8WT/K18R90C.
3. The presence of keratin filaments affects the motility of the mitochondria in MIN6 cells.
4. K18R90C mutation in keratin filament leads to structural changes in keratin structure and causes change in dynamics of mitochondria in MIN6 cells.
5. The presence/absence or mutation in K8 causes alteration in insulin production when stimulated with different glucose concentration in growth media.

3 AIMS

1. To determine the effect of the induced levels K8/K18 expression on the mitochondrial membrane potential.
2. To find the effect of keratin on mitochondrial motility in MIN6 cells.
3. To determine if mitochondria colocalize and interact with keratin filaments in MIN6 cells.
4. To determine the effect of K18R90C mutation in keratin filaments on mitochondrial morphology, distribution and differentiation in β-cells.
5. To determine the effect of absence/presence or mutations (K18 R90C and K8 G62C) of keratin filaments in insulin production due to glucose stimulation.

4 MATERIALS AND METHODS

4.1 Cell culture

4.1.1 Pancreatic β-cell line and MIN6 cell culture

Most cells have a definite life span of about 20-100 generations. But some of the genetically modified cells can produce immortal cell lines that can divide and grow for infinite number of generations (Freshney, 2005; Skelin et al., 2010). The key for the immortality of these cell line is in the mutation or deletion of the senescence genes, which causes shortening of the telomeres, essential for chromosomal functionality, on each cell division, or by overexpression of the oncogenes that can suppress the effect of the senescence gene (Skelin et al., 2010). Many mouse cell lines, developed from the tissues of liver, pancreas, blood, intestine or other body parts, were widely used in the drug testing and biological researches.

Primary β-cells do not grow easily in the culture. Numerous attempts have been made to establish a cell line that would mimic the insulin producing property of β- cells along with the same genotype (Skelin et al., 2010). Some of the cell lines originated from insulinoma in mice are MIN6, β-TC1, IgSV195 and β-HC. MIN6 cell line is one of the few cell line that actually produce insulin and respond to glucose in vitro (Ishihara et al., 1993). MIN6 cells are derived from transgenic mice that overproduce simian virus (SV) 40 large Tag antigen which ensures the continuous growth of the cells and induce the cancerous condition (Efrat and Hanahan, 1987). In normal pancreatic β-cells high level of tumor suppressing protein, p53 is found whereas it is highly checked in the RIP1-Tag transgenic mice. In RIP1-Tag transgenic mice, SV40 large T antigen is expressed under rat insulin promoter (RIP) (Efrat and Hanahan, 1987; Skelin et al., 2010). MIN6 cells grows in clusters and express GLUT2 and glucosekinase and responds to glucose stimulation within the physiological range in presence of nicotinamide (Miyazaki et al., 1990; Skelin et al., 2010).

MIN6 cells express only trace amount of K8/K18, which are the major keratin types found in β-cells. MIN6 cells were cultured in Dulbecco's modified Eagle medium 8DMEM) with 15% fetal bovine serum (FBS), 1% sodium pyruvate, 1% glutamax, 1% antibiotics streptomycin + penicillin (Pen/strep, Sigma Aldrich) and 0.54% β-mercaptoethanol added

fresh when using the media. Phosphate buffered saline (PBS) was used to wash the dead cells away. Trypsin containing 0.25% EDTA was used to detach the cells from the base of the cell culture flask. The cells were splitted when they were confluent enough in the cell culture flask (about 80%). The cells were incubated at 37^0C at 5% CO_2 level.

4.2 Transfection of keratin plasmids

Due to presence of only trace levels of keratin filaments in the MIN6 cells, K8 and K18 plasmids were transfected using electroporation transfection method. Electroporation is the most popular transfection method where high voltage electric impulses lasting for 20-30 miliseconds (ms) is given to the cells to introduce foreign plasmids or DNA to the cells. Electroporation produce transient and efficient transfection and expression of the transfected genes (Potter and Heller, 2003). When high voltage electric shocks is given to the cells, the pores at the cell membrane open up and the plasmids can enter the cytoplasm and finally to the nucleus where the plasmids integrate with the host for stable gene expression (Potter and Heller, 2003). For the transfection of keratin plasmids K8 WT, K18 WT, K8 tagged with yellow fluorescent protein (YFP), K18 R90C and K8 G62C plasmids were used. Electronic setup of 250 volts (V) along with capacitance of 875 μF was given through the electroporation device. Since the keratin filaments are heterodimers, different pairs of K8 variants (type-II) and K18 variants (type-I) were used for a single electroporation event. The total amount of keratin used in each transfection was 10 μg of plasmid each of type-I and type-II keratins. The Opti-MEM (1X) reduced serum media buffered with HEPES and sodium bicarbonate was used was used as the transfection media during the electroporation procedure. The transfected cells were incubated further for at least 48 -72 hours. The transfection efficiency for the keratin plasmids in the MIN6 cells was 10-15%. In this thesis work, the control groups for the experiments were not transfected and the normal untransfected MIN6 cells were used for the statistical analysis.

Table 1. Plasmids used for the transfection in the MIN6 cells for overexpression of different keratin IF types

Plasmid	Species	Concentration (µg/ml)
K8 WT	human	10
K8 YFP	-	10
K8 G62C	human	10
K18 WT	human	10
K18 R90C	mouse	10

4.3 Immunofluorescence staining

Immunofluorescence staining is a common biochemical technique used to label desired cellular proteins or molecules with fluorescent molecules or fluorophores. It allows the close visual observation of action of the particular antibody on the antigen under special fluorescence microscopes (Beutner, 1961)

4.3.1 Sample fixation

The MIN6 cells were plated on sterile cover glasses with the thickness of 0.17 mm along with 1 ml of DMEM media solution in a 24-well cell culture plates and were allowed to incubate for 48-72 hours. After washing the cells with PBS solution for 2-3 times, 1% paraformaldehyde (PFA) was introduced for the fixation of the MIN6 cells. PFA was kept for 20 minutes at room temperature and was then removed and again washed with PBS three times at 5 minutes interval and the cells were stored with 1 ml PBS at 40^0C temperature.

4.3.2 Immunofluorescence staining

Indirect immunofluorescence technique was used to stain the cells where the primary antibody binds with target protein and the primary antibody is bound to a fluorophore molecule. The fluorophore molecules are excited by the light or radiation of a certain wavelength and in turn emits light/radiation of higher wavelength that possess lower energy levels than the incident wave and is detected and visualized with the help of fluorescence microscope (Robertson and Kertesz, 1975).

After the fixation of the MIN6 cells with 1% PFA, cells were washed three times with PBS and the cover glasses were transferred to moisture chamber with a sterile forceps where the

entire staining procedure is performed. The cells were treated with NP-40 (nonyl phenoxypolyethoxylethanol, pH 7.1) in PBS to increase the permeability to the antibodies for five minutes. Then the coverslip glass was washed three times with PBS. The blocking step was done with the buffer A solution (2.5% bovine serum albumin (BSA, Sigma Aldrich) in PBS) for 20 minutes at room temperature. Then it was removed. To avoid unspecific binding of the primary antibody, buffer C was introduced (2.5% BSA with 2% donkey serum and 2% goat serum in PBS) and incubated for 10 minutes at room temperature. Then the samples were incubated with primary antibody overnight (table 1).

Table 2. Primary antibodies used for immunofluorescence staining

Target protein	**Antibody name**	**Host**	**Concentration**	**Manufacturer**
K8	Troma I	Rat	1:500	Developmental Studies Hybridoma Bank
Tom20	TOM20	Rabbit	1:500	Santa Cruz Technologies
Insulin	Insulin	Rabbit	1:500	Santa Cruz Technologies

The primary antibodies were diluted with Buffer C. Different primary antibodies were used to detect different protein sets according to the aim of the experiments. Troma I was used to bind with K8 protein and used in all the experiments where keratin immunofluorescence was done. TOM20 antibody binds with the TOM20 receptor at the outer membrane of mitochondria and used alongside Troma I to examine the relationship between keratin and mitochondria. Similarly insulin antibody was used alongside Troma I to find the relationship between the keratin and insulin vesicles in the MIN6 cells. The staining controls were incubated with Buffer C solution without the primary antibody.

After the incubation with the primary antibodies, the samples were washed three times with PBS to remove any unbound primary antibody and again blocked with Buffer C for 10 minutes before introducing to the secondary antibodies and incubating in room temperature for 30 minutes. The secondary antibodies were diluted with Buffer C. Table 2 shows the different secondary antibodies used in the experiments. Alexa 488 have peak excitation and emission wavelengths of 493 nm and 519 nm respectively. Similarly Alexa Fluor 568 binds

with primary antibody with rat host and has peak excitation and emission wavelengths of 578 nm and 603 nm respectively. Alexa Fluor 488 and 568 was used in pairs to stain keratin and TOM20 or keratin and insulin. The excitation and emission spectra didn't interfered or had fluorescence crosstalk.

Table 3. Secondary antibodies used for staining the different keratin filaments and mitochondria

Antibody	**Host**	**Concentration**	**Manufacturer**	**Product number**
Anti-rabbit Alexa® 488	Donkey	1:200	Life technologies	A21206
Anti-rat Alexa® 568	Donkey	1:200	Life technologies	A11077

After incubating the sample with secondary antibody, the sample was washed three times with PBS and a nuclear marker, DRAQ5, was introduced and incubated for 5 minutes. DRAQ5 is a nuclear stain. DRAQ5 was diluted with PBS for the use on the samples. Its excitation and emission wavelengths are 647 nm and 681 nm respectively. Abberior STAR 488 was used for the STED microscopy due to its higher photostability and less photobleaching features. DRAQ5 was used along the Alexa Flour 568 during sample preparation for the STED microscopy. The excitation wavelength used for STED was 488nm while the depletion during the STED microscopy is at approximately 590 nm.

Table 4. Nuclear marker used in the staining procedure

Nuclear Marker	**Name**	**Concentration**	**Manufacturer**
DRAQ5	4084S	1:2500	Cell Signaling, Danvers, MA, USA

After treating the sample with DRAQ5 the cover glasses were mounted on the glass slides with a drop of mounting media, Prolong Gold (P36930, Invitrogen). The function of the mounting media like Prolong gold is to help to glue the cover glass well to the glass slide and to reduce the rate of photo bleaching of the fluorophores involved in the immunofluorescence procedure.

4.4 Glucose stimulation of MIN6 cells and insulin production

To investigate the effect of different levels of glucose stimulation on MIN6 cells and its insulin secreting pattern, various level of D-glucose (Sigma-Aldrich) was given to the MIN6 cells to check the variation or change in number of insulin vesicles in MIN6 cells over expressing wild type keratins (K8WT/K18WT), mutant keratins (K8WT/K18R90C and K8G62C/K18WT) and keratin-negative MIN6 cells. The cells were grown in normal DMEM media with 25 mm glucose in 24 well plates on cover glasses. The media was removed and washed two times with PBS and the cells were then incubated with Krebs Ringer Bicarbonate (KRB) buffer with 5 mM for 30 minutes to reset or stop the glucose production from the MIN6 cells. Then two different glucose levels with two different times were given for glucose stimulation to the MIN6 cells making a total of 4 cases (5 mM/5mins, 5 mM/180mins, 30 mM/5mins and 30 mM/180mins). The cells were immediately fixed after their desired stimulation time with 1% PFA. Immunofluorescence staining for insulin, keratin and nuclei was done for the fixed cells followed by confocal microscopy with Leica TCS SP5 Matrix. KRB buffer and D-glucose solution were freshly prepared for the experiment.

4.5 Microscopy

4.5.1 Bright field and fluorescence microscopy

The cells cultured for the experiments were checked once every two days by using an inverted light microscope using phase-contrast illumination. Leica DN IL with features like phase contrast illumination was used with different objectives, 10X, 20X and 40X. During the inspection, the confluency of the cells on the cell culture flasks was routinely checked along with normal/abnormal growth patterns. Bacterial or yeast contamination was also checked during the microscopy sessions.

Likewise, Leica DM IRBE fluorescence microscope was used for analyzing the fluorescence of the K8 YFP transfected cell cultures for stable cell line experiment and after the immunofluorescence staining before going to the confocal microscope.

4.5.2 Confocal fluorescence microscopy

The laser scanning confocal microscope (LSCM) is widely used in medical and molecular biological researches due to the comparative higher resolution. The confocal microscope

consists of two confocal pinholes places at confocal planes, which highly reduce the background illumination of the sample, and very thin layer of sample can be observed with the microscope. Since the out-of-focus light is excluded, the optical resolution and contrast is considerably higher than the normal fluorescence microscope and narrow depth of field can be achieved with much better signal-to-noise ratio. Lasers like Argon laser (488 nm, 514 nm), Argon-Krypton (488nm, 568 nm, 647 nm) and Helium-Neon (633 nm) lasers are the most commonly used lasers. The lasers scan the sample one point at a time and the whole sample is scanned in raster pattern. The photomultiplier tube (PMT) and charge coupled device (CCD) cameras are the most commonly used detectors (Matsumo, 2003). The optical filters are the wavelength specific components which transmit, blocks or reflect certain wavelength of light and it is present in both excitation and emission parts, complementing to each other, in the LSCM.

The confocal microscope Leica TCS SP5 Matrix, HCS A was used for the confocal microscopy of all the samples in all the experiments. 10X (air), 40X (air) and 63X (oil) objectives were used for the imaging of the samples while 63 X oil objectives was used for the analysis of the samples. The Argon-Krypton and Helium-Neon lasers were used in the microscope in the experiments for excitation at 488 nm (for Alexa Fluor 488), 568 nm (for Alexa Flour 568) and 647 nm (for DRAQ5) was used in the keratin, TOM20 and insulin based experiments. Similarly, during the live cell imaging of the MIN6 cells with TMRE and keratin, excitation at 549 nm and 488 nm was used respectively.

4.5.3 Stimulated Emission Depletion Microscopy (STED)

The highest resolution of the confocal microscope today with optimum condition (numerical aperture (NA) =1.40, wavelength (λ) = 550 nm) is 200 nm based on the Rayleigh's principle of resolution. The resolution is calculated by 0.61*λ/NA. This resolving power of the microscope is limited by the diffraction of the light causing the light to spread in a plane space known as point spread function (PSF). It is determined by the wavelength and the numerical aperture of the optical system (Olympus, 2017). STED technology has improved the resolution of the optical system by overcoming the diffraction limit by minimizing the spreading of the fluorescence emission from the sample. According to the normal fluorescence principle, which is followed by all the fluorescence and confocal microscopes, when a fluorophore is excited by a wavelength of light, the electron

at the outer orbit goes from the ground state S0 to an excited unstable state S1. When the electron at S1 returns back to the ground or stable state, it releases a photon, causing the fluorescence effect. In STED, the returning electrons are forced to relax at the excited state which causes red shift in the emission. This stimulated photon is ignored and the remaining fluorescence obtained is used for image acquisition. The resolution is highly increased due to lower PSF. Instead of one laser excitation source normally used in confocal microscope, STED microscope have another laser source which gives 'STED' beam that is usually doughnut-shaped pulsed beams which suppressed or depletes the surrounding electrons except the central portion. Here a doughnut-shaped pulse is longer wavelength and it bleaches the fluorophores to the ground state cuts off the surrounding fluorophores' emission and only the central fluorophores are able to emit the fluorescence. Hence, very narrow PSF can be achieved and the super resolution beyond the diffraction limit can be achieved.

Leica TCS STED microscope was used for taking images for the visualization of the colocalization of mitochondrial TOM20 protein with the keratin filaments due to the high resolution of STED microscope. Normal immunofluorescence staining protocol was followed for the STED microscopy with the exception of usage of Abberior STAR 488 instead of Alexa Fluor 488 for TOM20.

4.6 Cell sorting

Flow cytometry, in biotechnology, is a widely used method for analysis of populations of cells. The cells can be sorted according to their size or fluorescence emissions from a heterogeneous cell population. In flow cytometry, the specific proteins or ligands in the cells are labeled with fluorescent antibodies and single cell suspension is made which runs through the flow cytometer that can differentiate the fluorescent and non-fluorescent cell and hence sorted accordingly. Similarly the cells can also be sorted according to the fluorescence intensity of the fluorescent proteins.

Flow cytometry can be used in counting the cells that are transfected with fluorescent protein. For the development of stable MIN6 cell line that overexpresses K8 YFP and K18 proteins, we transfected these keratin plasmids (10 μg each) and let them incubate for 72 hours in a cell culture flask at 37ºC. When they had attached to the cell culture flask, the cells were observed with the Leica DM IRBE inverted microscope for the fluorescent

proteins. After that, they were detached using trypsin with 0.25% EDTA and transferred to 5 ml Falcon round bottom test tube for the flow cytometry. BD FACS Aria IIu Cell Sorter was used for the separation of the transfected and non-transfected cells. The transfected cells were collected in the 96-well cell culture plate with pre-heated DMEM with 15% FBS, 1% sodium pyruvate, 1% glutamax, 1% antibiotics streptomycin + penicillin (Pen/strep, Sigma Aldrich) and 0.54% β-mercaptoethanol freshly added. 64 wells were seeded with fluorescent cells. Approximately, 500-1000 cells were seeded in each well. The cells were further allowed to grow undisturbed for next 72 hours and then checked every fourth day for increase or decrease in fluorescence with the Leica DM IRBE inverted fluorescent microscope. The MIN6 cells were tested for mycoplasm contamination and were tested negative. Similarly, flow cytometry was also used to analyze the transfection efficiency K8YFP and K18WT by electroporation and was found to be 11%

4.7 Live Cell Imaging for mitochondrial membrane potential (ΔΨm) measurement and mitochondrial motility analysis

MIN6 cells transfected with K8 YFP and K18 WT were grown in cell culture for 72 hours after the transfection in a 35 mm glass bottom petri dish (MatTek Corporation, Ashland, MA, USA; glass bottom thickness=0.17 mm) and tetramethylrhodamine ethyl ester (TMRE) staining was done for mitochondrial membrane potential analysis. For TMRE staining, imaging buffer solution (IBS) was prepared by adding 30 ml Krebs-Ringer Bicarbonate (KRB) Buffer and 150 µl of 1M D-Glucose (Sigma-Aldrich). TMRE stain solution was prepared by dilution 2.5 µl TMRE (stock 200 mM) and 5 ml IBS making a final solution of 100 nM. Before the staining, the cells were washed two times with 1 ml IBS. Then 2 ml of TMRE solution was added to the cell culture plate and incubated for 20 minutes at 37ºC. The TMRE stain solution was removed after the incubation and was replaced with 2 ml IBS and was taken to the Leica TCS SP5 Matrix confocal microscope for the live cell imaging. KRB buffer and D-Glucose were freshly prepared. For mitochondrial motility analysis, the short exposures in every 10 seconds were given for two minutes.

The Leica TCS SP5 Matrix confocal has a special chamber with 35 mm petri dish compatible stage that can maintain 37ºC temperature, 5% CO_2 level and appropriate humidity level for live cell imaging procedure to prevent the cells from environmental

shock for many hours. Images were taken with 10X and 63X (used for the analysis purpose) objectives. Two channels were used with the excitation frequency of 488nm (Argon laser) for YFP tagged K8 and 543 nm (HeNe laser) for TMRE. By using LAS software from the microscope, sequential scans of the sample were done to acquire images.

4.8 Image processing and Statistical Analysis

Image processing was done mostly with Image J software and partially with Bitplane Imaris while statistical analysis were done using Prism-graphpad software.

4.8.1 Mitochondrial membrane potential (ΔΨm)

The membrane potential between the matrix and the inner-membrane space in the mitochondria was measured using average mean intensity values by manually drawing region of interest (ROI) around the mitochondria while for keratin filaments, Corrected Total Cell Fluorescence (CTCF) was taken into account for the comparative analysis between the high keratin concentrated MIN6 cells and low keratin concentrated MIN6 cells. Median was considered for the separation of the higher or lower keratin concentration levels and hence the results were divided into two groups, higher keratin concentrated cells and lower keratin concentrated cells. Median was chosen instead of mean value as to eliminate the influence of the spiked or extreme values shown by some cells.

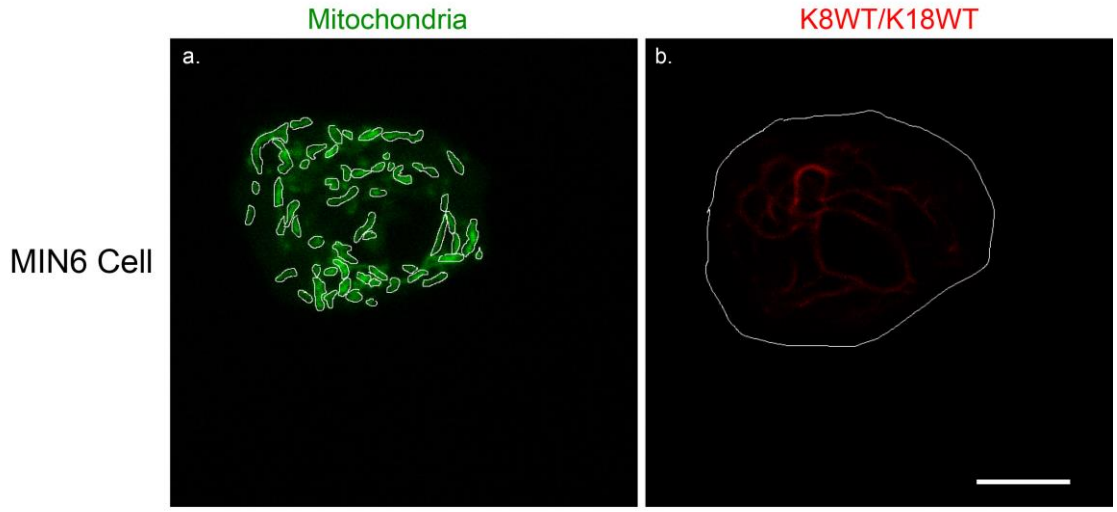

Figure 11. (a) Calculation of mean fluorescence intensity of mitochondria (green). Several ROIs from the mitochondria were drawn to measure the mean fluorescence intensity. (b) Calculation of CTCF of keratin IF (red). The whole cell was taken into account for the calculation of CTCF of keratin IF where K8 was tagged with YFP (white circle in b.).

4.8.2 Mitochondrial Motility

Mito-tracker plugin, which is built in Image J software. The time lapse image series was taken every ten seconds for two minutes was used for tracking the head/tail or the extreme side of the elongated mitochondria. The mitotracker plugin was used to trace the path travelled by the mitochondria which eventually gave the velocity of the mitochondria. Hence, mitochondrial motility was calculated.

4.8.3 Colocalization analysis

Colocalization represents the interaction of various proteins in the cells. Colocalization between the keratin filaments and mitochondria was analyzed using Image J software while Bitplane Imaris was also tested for colocalization evaluation. COLOC-2 plugin in Image J software was used for finding the colocalization of the TOM20 protein in the outer-membrane of the mitochondria and keratin filament (K8/K18). After taking images from Leica TCS SP5 Matrix confocal and Leica TCS STED microscope the correlation between the red (keratin) and green (TOM20 of mitochondria) channel were analyzed through the COLOC-2 plugin in Image J. Different correlation coefficients like Pearson's coefficient of correlation and Mander's coefficient were obtained where Pearson's coefficient of correlation was considered for evaluation (Mukaka, 2012). It ranged from -1 to +1 where +1 represents perfect positive correlation, -1 represents perfect negative correlation and 0 means no correlation.

4.8.4 3-Dimensional projections of mitochondria and insulin

The outer membrane protein, TOM20 was used as the marker for the mitochondria. After the immunofluorescence staining, Z-stack images were acquired from the Leica SP5 matrix laser scanning confocal microscope. Then 3D surface rendering was done with the Bitplane Imaris software where 3D-projections of the mitochondria were created for each cells of the different groups of cells. After the construction of the 3D images, the 3D projections of the mitochondria were scored by three people by blind on the score of 1-5 where 1 is represented most clumped mitochondria in a cell and 5 represented most dispersed and diffused mitochondria in a cell. This analysis method was used in comparative analysis of structure of mitochondria in presence of wild type keratin (K8/K18) and mutant keratins (K8WT/K18R90C and K8G62C/K18WT).

4.8.5 Mitochondria and Insulin vesicle counting

After the immunofluorescence staining for TOM20 and different types of keratins in MIN6 cells, 2D images were taken from the confocal microscope and further processed with Image J and Bitplane Imaris for the counting of the mitochondria. At first, the individual cells were cropped out from the clusters of cells, which is normal in healthy MIN6 cells. After cropping the individual cells, channel separation was done as the immunofluorescence was done for three fluorophores. We isolated the TOM20 channel for mitochondria. After channel isolation, the image was imported to Bitplane Imaris and spot-feature was applied which counts the fluorescent areas and tags them as 'spots'. The thresholds were manually optimized for proper and correct recognition of fluorescent signals from the image. The results were stored and compared among the MIN6 cells overexpressing wild type keratins (K8WT/K18WT), mutant keratins (K8WT/K18R90C and K8G62C/K18WT) and keratin negative MIN6 cells.

Similar procedure was followed for counting of the insulin vesicles with the normal glucose level cells as well as the MIN6 cells stimulated with different concentration of glucose levels. The results were also compared with MIN6 cells over expressing wild type keratins, mutant keratins and keratin negative MIN6 cells.

To count mitochondria and insulin vesicles in MIN6 cells, the numbers were converted to the value in terms of per unit area. One unit area represents one micrometer square ($1\mu m^2$). Since the size of cells is not consistent with each other, the number or mitochondria and insulin vesicles might be influenced by the area of the cell. So, I calculated the number of mitochondria or insulin vesicles as per unit area instead of per unit cell. During the calculations, the number of mitochondria or insulin vesicles are divided by the area of the cell. This process was done for large number of the cells and the average was calculated from all the cells considered for the calculation. For example, if the area of a MIN6 cell is 150 square units with 75 mitochondria, then there will be 0.5 (75/150) mitochondria per unit area for that cell. When more cells are taken, average of the per unit area values are calculated for the final result. For instance, if there are five cells with 0.5, 0.2, 0.6, 0.8 and 0.5 mitochondrial count per unit area, then the average mitochondrial count for this group of cells will be 0.52 {(0.5+0.2+0.6+0.8+0.5)/5}. Hence, the Y-axis in the graphs in figure

16, 17 and 19 represents the mean ratio of the number of mitochondria or insulin vesicles and the cell area of that particular cell.

4.8.6 Statistical analysis

The statiscical analysis for all the results were done with two tailed Student's test and one-way Anova with Bonferronis' post hoc test were done from Graphpad Prism software. P values * = $p<0.05$, ** = $p<0.01$ and *** = $p<0.001$ were considered significant with 95% confidence interval.

5 RESULTS

5.1 Mitochondrial motility is influenced with the presence of keratin IF

To find out if the presence of keratin filament increase or decrease the speed of mitochondrial in MIN6 cells, the movement of mitochondria were tracked and analysed in this experiment. Mitochondrial motility was analyzed in MIN6 cells where the mitochondria were labeled with TMRE using live cell imaging in the Leica SP5 matrix LSCM. The individual mitochondria were manually tracked for 2 minutes (figure 12a). The motility of the mitochondria in the untransfected MIN6 cells (which are almost keratin null) were almost double the speed of the mitochondria in K8/K18 overexpressing MIN6 cells (figure 12b). This result suggested that the presence of keratin in MIN6 cells resulted in less motility (about half) of the mitochondria and keratin filaments have a dynamic role in mitochondrial functionality in the MIN6 cells.

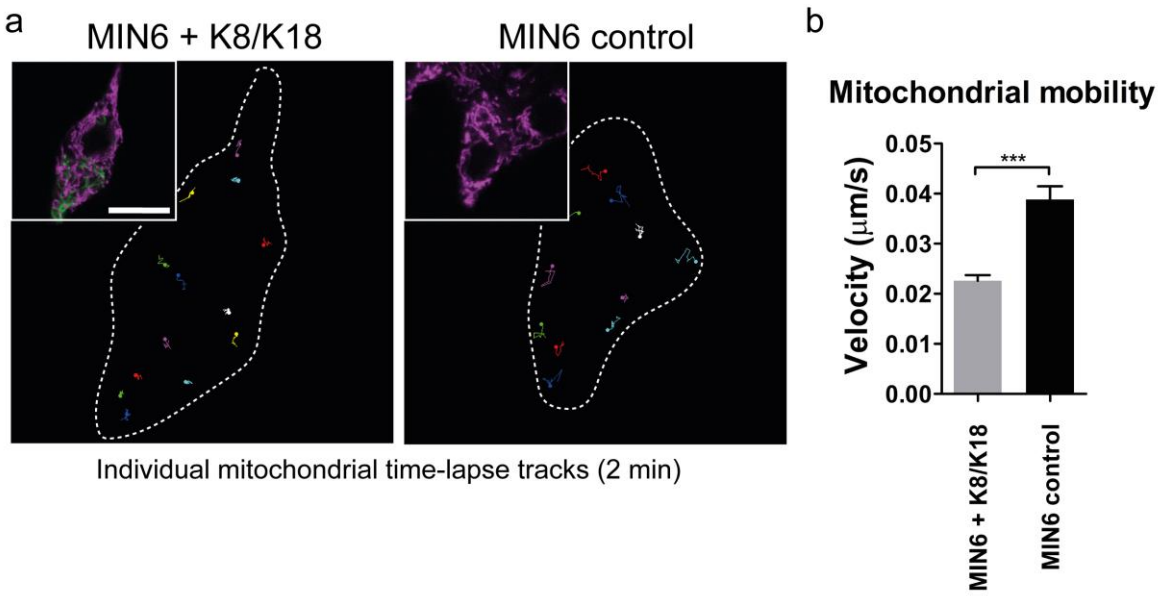

Figure 12. Mitochondrial motility decrease by almost half the speed due to presence of K8WT/K18WT. (a) Tracking movement of the individual mitochondria (magenta) in the MIN6 cells. The movement of mitochondria were tracked with the help of time lapse images from the Leica SP5 matrix confocal microscope where one image was taken every ten seconds for two minutes. Using Mitotracker plugin in ImageJ software, path of the mitochondria, represented by various colors, were traced and its velocity was calculated. (b) The average velocity of mitochondria in MIN6 cells overexpressing K8/K18 was about half the velocity of the mitochondria in untransfected MIN6 cells which are almost keratin null. Data is shown as average ± SEM. *** = $p < 0.001$. Scale bar = 10 μm.

5.2 Colocalization of keratin filaments and mitochondrial TOM20 was not seen using Pearson's coefficient of correlation analysis of 2D images

To determine a potential colocalization of mitochondrial TOM20 with keratin filaments, 2D images were taken from the Leica SP5 matrix confocal microscope with separate channels for TOM20 and keratin filaments. The samples for microscopy were prepared from MIN6 cells which were fixed and stained using immunofluorescence technique. The sites of colocalization were grey in color (mixture of green and magenta, using look up table (LUT) from Image J, gives grey when overlapped with each other) and can be faintly seen in the images (figure 13A). The images were then analyzed using the Image J software and built-in COLOC2 plugin was used for calculation of Pearson's Coefficient of Correlation (PCC). It gave the coefficient values from -1 to 0 to +1, 0 being absence of correlation while values towards +1 and -1 gave positive and negative correlation of the K8 and mitochondrial TOM20. Mitochondrial TOM20 and keratin filaments did not show any significant colocalization showed by the PCC in this experiment. The correlation coefficient was found to be about 0.04 for mitochondrial TOM20 and keratin K8 in the MIN6 cells overexpressing K8WT/K18WT (figure 13B).

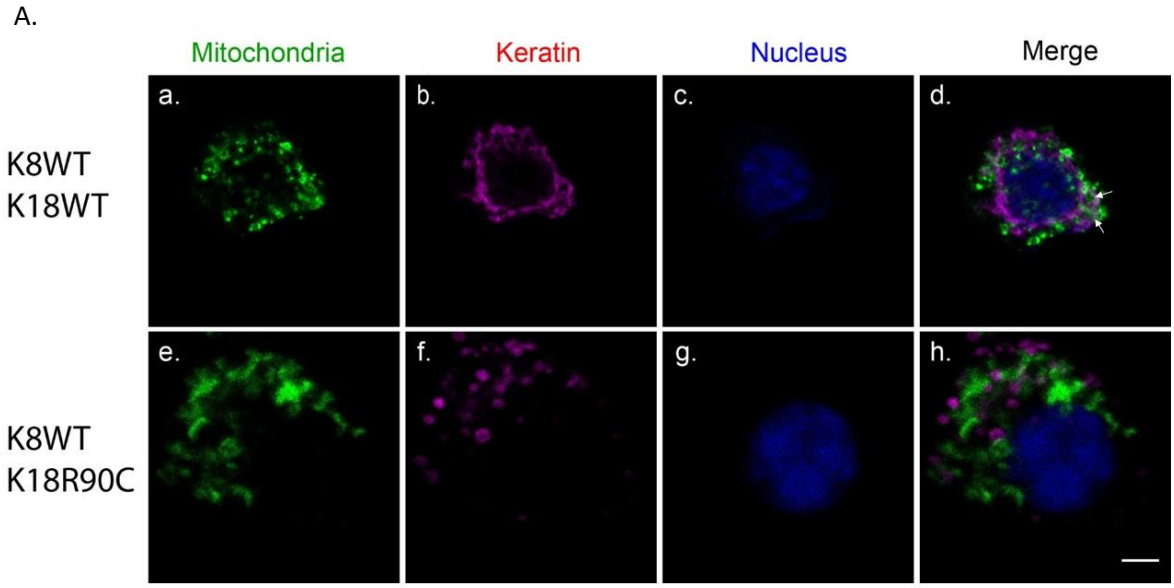

B.

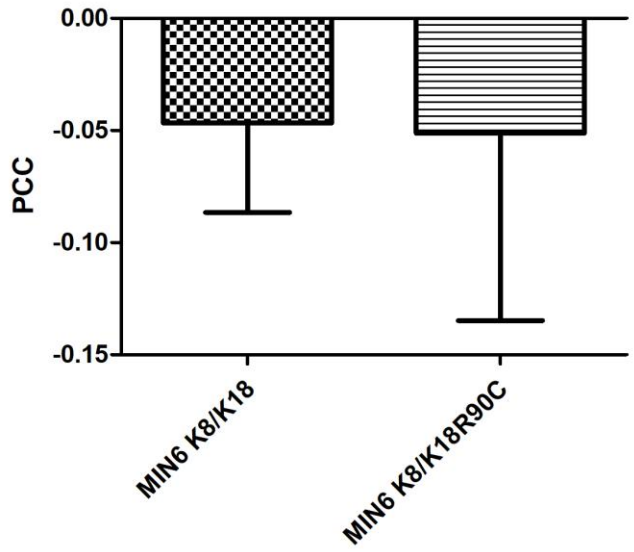

Figure 13. Colocalization of keratin K8 and mitochondrial TOM20 is not statistically significant. (A) Colocalization of mitochondria (green) on WT and mutant keratin IF (magenta). The small grey areas (pointed by arrows) indicate the colocalized points of mitochondria and keratin IF. Nuclei are indicated in blue. Scale bar= 5 µm. (B) The colocalization of mitochondria and keratin IF is inconclusive from the Pearson's coefficient of correlation (PCC) value. The images based on which the PCC were calculated were from the confocal microscope with highest resolving power upto 200 nm. Hence, finer details of the colocalization points were not observed in the images.

5.3 Fragmentation levels of mitochondria was found to be significantly different in MIN6 cells overexpressing the WT and mutant keratin overexpressing MIN6 cells and control group

In order to study about the fragmentation level of mitochondria in MIN6 cells in presence, absence or mutation of keratin, 3D stack images of mitochondria in MIN6 cells were taken by Leica SP5 Matrix LSCM and surface rendering was done using Bitplane Imaris software (figure 14A). These 3D surface rendered images were then scored by three individuals and scored from 1-5, where 1 was the lowest fragmentation level and 5 was the highest fragmentation level (figure 14B). It was found that the fragmentation level of mitochondria was highest with MIN6 cell control group that doesn't overexpress keratin filaments and with MIN6 cells overexpressing K8G62/K18WT keratin (figure 14B). The least level of mitochondrial fragmentation was found in the MIN6 cells overexpressing

K8WT/K18R90C while the MIN6 cells overexpressing K8WT/K18WT had medium level of mitochondrial fragmentation (figure 14B).

Comparatively, the mitochondrial fragmentation was seen significantly higher in the control MIN6 cells and K8G62C/K18WT overexpressing MIN6 cells compared to the MIN6 cells overexpressing K8WT/K18WT and K8WT/K18R90C (figure 14B).

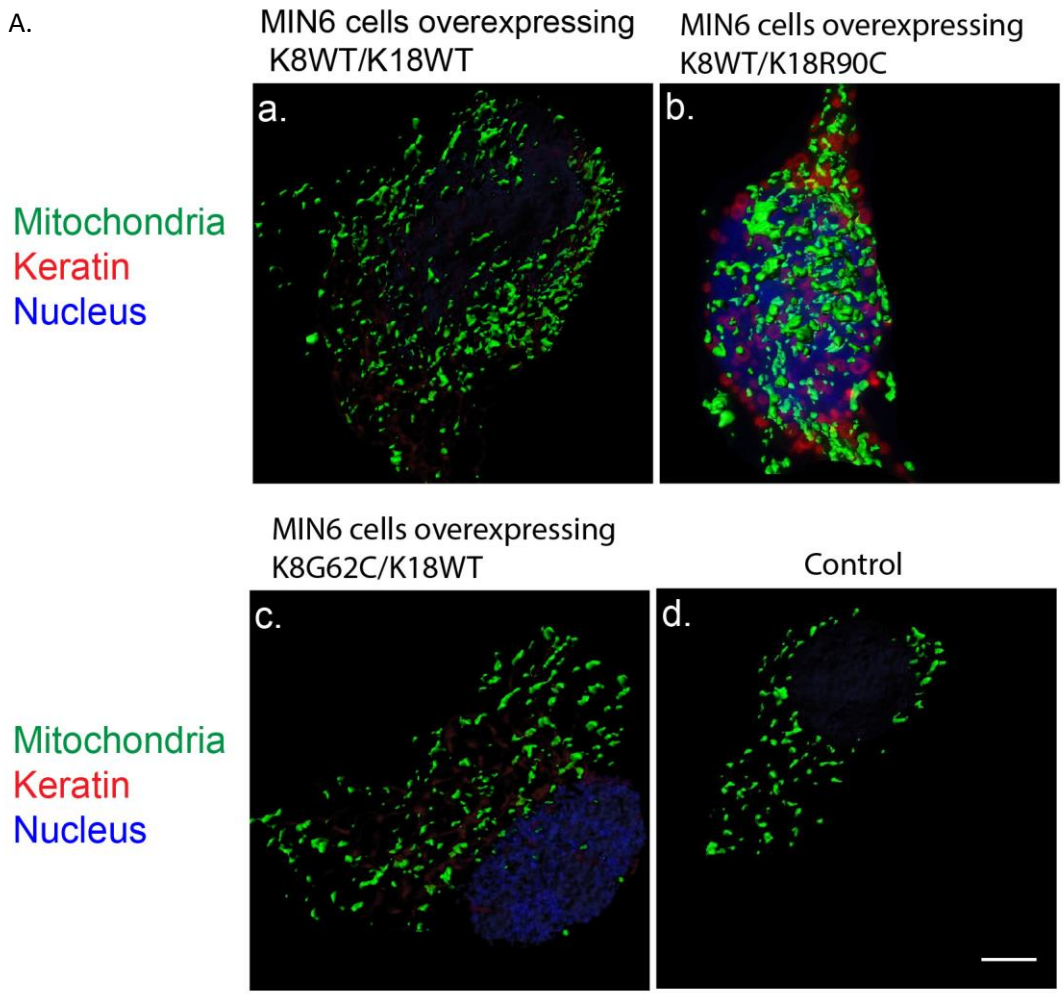

B.

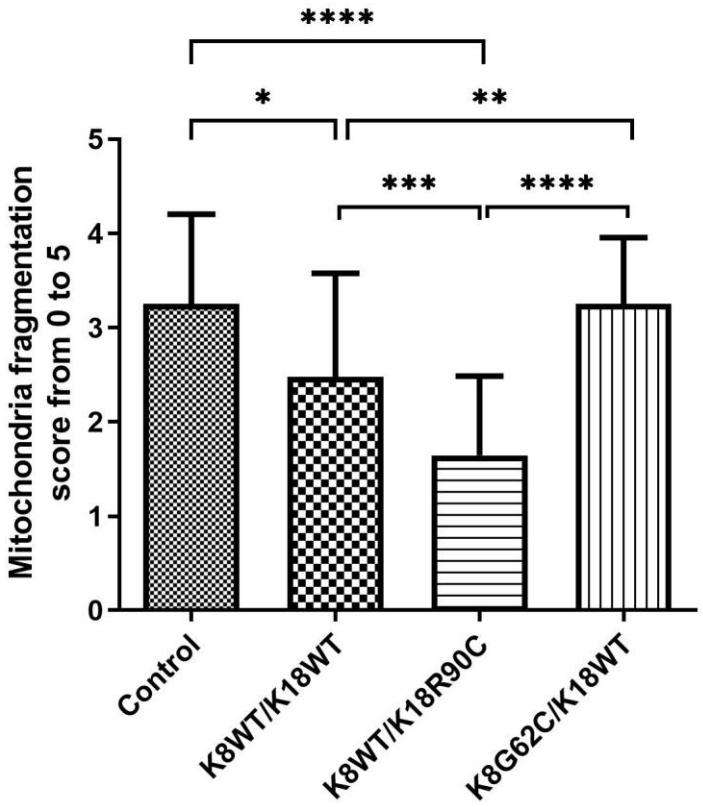

Figure 14. Mitochondrial fragmentation is highest in untransfected MIN6 cells and MIN6 cells overexpressing K8G62C and lowest in MIN6 cells overexpressing K18R90C. (A) 3D rendered surface image of mitochondria (green), different types of keratin IF (red) and nuclei (blue) to show the fragmentation levels of mitochondria in MIN6 cells overexpressing different keratin types (a) 3D rendered image of mitochondria in a MIN6 cell overexpressing K8WT/ K18WT. (b) 3D rendered image of mitochondria in a MIN6 cell overexpressing K8WT/K18R90C. (c) 3D rendered image of mitochondria in a MIN6 cell overexpressing K8G62C/K18WT. (d) 3D rendered image of mitochondria in WT MIN6 cell which is almost keratin null. Scale bar = 5µm. (B) Mean scores of the 3D-rendered surface images from the scale of 0 to 5 step scale where 0 represents the least degree of fragmentation while 5 represented highest degree of fragmentation ± SD. The WT MIN6 cells had highest fragmentation score of mitochondria along with MIN6 cells overexpressing K8G62C/K18WT while MIN6 cell overexpressing K8WT/K18R90C had the lowest fragmentation score. MIN6 cells overexpressing K8WT/K18WT had medium fragmentation scores. Statistical significance was calculated with 2-tailed student's t-test where * = $p<0.05$, ** = $p<0.01$, *** = $p<0.001$ and **** = $p<0.0001$.

5.4 No significant difference in mitochondrial ΔΨm was found in MIN6 cells expressing different levels of keratin

MIN6 cells overexpressing different levels of YFP-tagged K8WT and K18WT (as determined by YFP fluorescence intensity/cell) were used to determine the effect of the level of overexpression of keratin on the ΔΨm. TMRE was used as the membrane potential marker and live cell imaging was done in the temperature, humidity and CO_2 level controlled live cell imaging chamber of the Leica SP5 matrix laser scanning microscope. Average mean values of the mitochondrial membrane fluorescence from TMRE probe and corrected total cell fluorescence (CTCF) of the YFP tagged K8 were calculated for each of the 26 cells analyzed and the resulting data was divided into two groups separated by median value of the data series (figure 15). Total of four possible outcomes were organized and number of events were counted for each outcome. There were 8 events where there were high keratin level and high ΔΨm, 6 events with high keratin level and low ΔΨm, 7 events with low keratin level and high ΔΨm and 6 events with low keratin level and low ΔΨm. Thus, the results (figure 15) showed that there was no major difference with the ΔΨm based on the keratin level in the MIN6 cells and that the amount of keratin in the MIN6 cells have negligible impact on the mitochondrial functionality.

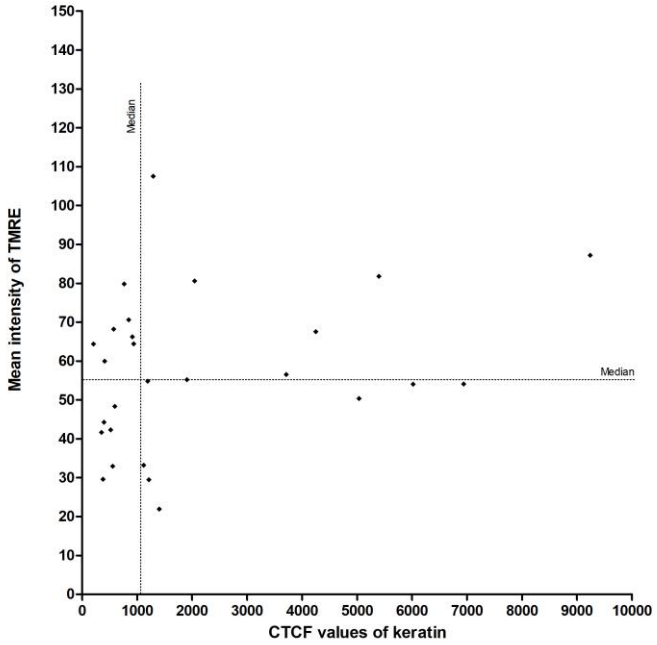

Figure 15. There was no major difference in mitochondrial potential due to varying levels of K8YFP/K18WT in MIN6 cells. Mean intensity of TMRE represents the mean fluorescence intensity from the TMRE probe of mitochondria while the CTCF of keratin represents the fluorescence intensity from YFP tagged K8 in the Min6 cells. The median lines divide the axes into higher value and lower value groups. Distribution of occurrence of various outcomes showed that there were 8 events with high keratin and high ΔΨm, 6 events with high keratin and low ΔΨm, 7 events with low keratin and high ΔΨm and 6 events with low keratin and low ΔΨm.

5.5 Number of mitochondria is higher in MIN6 cells overexpressing WT than the control and MIN6 cells overexpressing mutant keratin (K18R90C)

In order to determine the number of mitochondria in untransfected MIN6 cells and MIN6 cells overexpressing WT and mutant variants of keratin, this experiment was performed. After immunofluorescence staining of the MIN6 cells, Leica SP5 matrix microscope was used to acquire 3D stack images. The acquired images were then analyzed using Image J and Bitplane Imaris for 3D surface rendering to get the 3D representation of the mitochondria and keratin filaments. Spot counting was done to count the number of mitochondria. Since the size of the cells differ from each other, there is possibility of biasness if the counting is done in terms of cells. So, the number of mitochondria was divided by the cell area to acquire 'mitochondrial count per unit area' and the mean of

mitochondrial count per unit area is shown as the result for this experiment (figure 16). The results showed that the number of mitochondria was higher in MIN6 cells overexpressing WT K8/K18 compared to control group MIN6 cells which lacks keratins and MIN6 cells overexpressing K8WT/K18R90C (figure 16).

The K18R90C mutation which causes disruption of keratin filaments leads to lower number of mitochondria and is comparable to MIN6 cells without keratin filaments.

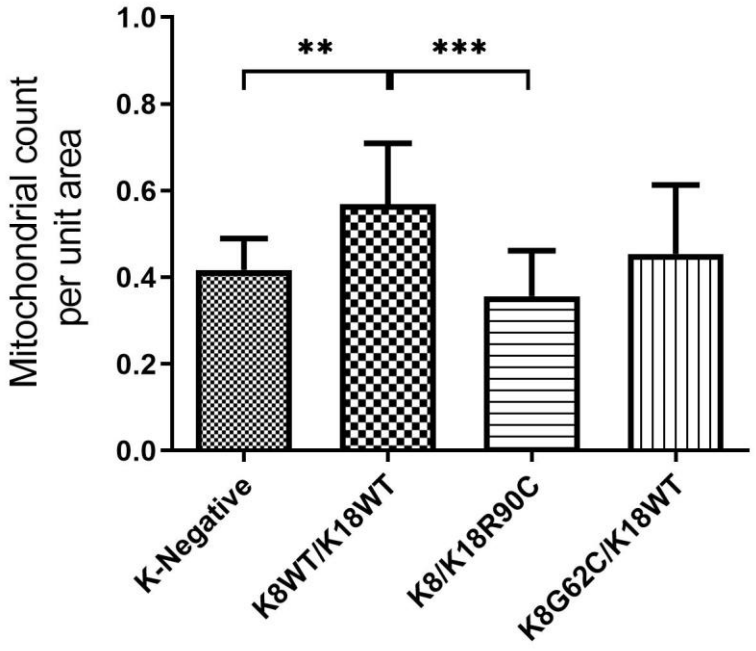

Figure 16. Min6 cells overexpressing K8WT/K18WT had the highest number of mitochondria per unit area of the cell compared to the untransfected MIN6 cells and MIN6 cells overexpressing K18R90C. The result is represented as the mean of the mitochondrial count per unit area of the MIN6 cells. Here, the unit area represents cell area of 1μm^2. There is significant difference in number of mitochondria per unit area between the control WT MIN6 cells and MIN6 cells overexpressing K8WT/K18WT. Likewise, there is also a significant difference in mitochondrial count between WT keratin overexpressing MIN6 cells and mutant keratin (K18R90C) overexpressing MIN6 cells. Statistical significance was calculated with 2-tailed student's t-test where * = $p<0.05$, ** = $p<0.01$ and *** = $p<0.001$.

5.6 Number of insulin vesicles is higher in control MIN6 cells compared to MIN6 cells overexpressing WT keratin (K8/K18) and mutant keratin K18R90C

In order to determine the number of insulin vesicles in untransfected MIN6 cells and MIN6 cells overexpressing WT and mutant variants of keratin, this experiment was performed. After immunofluorescence staining of the MIN6 cells, Leica SP5 matrix microscope was used to acquire 3D stack images. The acquired images were then analyzed using Image J and Bitplane Imaris for 3D surface rendering to get the 3D representation of the insulin vesicles and keratin filaments. Spot counting was done to count the number of mitcondria. Since the size of the cells differ from each other, there is possibility of biasness if the counting is done in terms of cells. So, the number of insulin vesicles was divided by the cell area to acquire 'insulin vesicle count per unit area' and the mean of insulin vesicle count per unit area is shown as the result for this experiment (figure 17). It was found that untransfected MIN6 cells (control group), which are almost keratin null, had highest number of insulin vesicle per unit area of the cell while the keratin filament disrupting mutation K18R90C had lowest number of insulin vesicles per unit cell area. Similarly, the MIN6 cells overexpressing WT keratins had lower amount of insulin vesicles compared to untransfected MIN6 cells (figure 17). Interestingly, the MIN6 cells that overexpressed K8G62C had higher number of insulin vesicles compared to WT and K18R90C overexpressing MIN6 cells. It seems that the disruption of keratin filaments in K18R90C overexpressing MIN6 cells might have significant impact in production of insulin and significant loss in number of insulin vesicles.

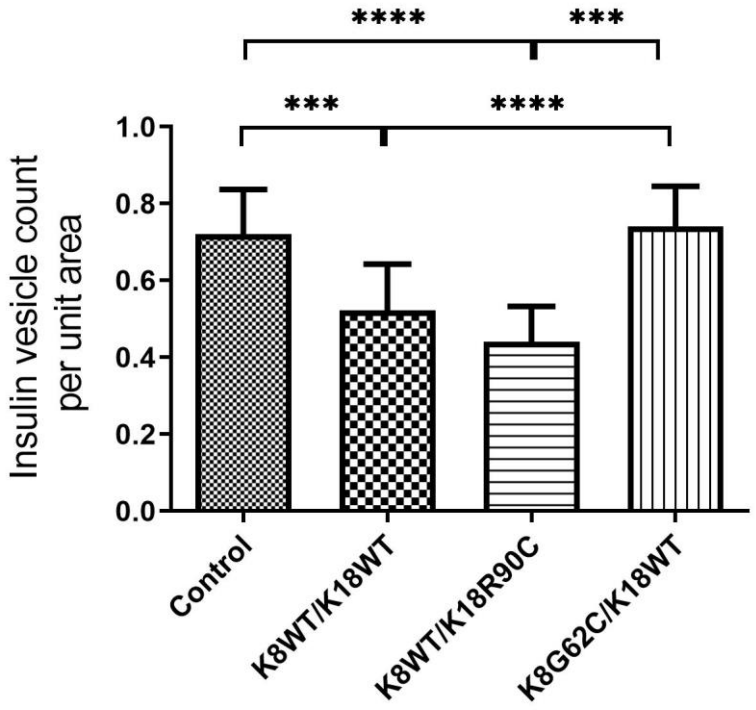

Figure 17. Untransfected MIN6 cells and MIN6 cells overexpressing K8G62C had highest number of insulin vesicles while the MIN6 cells overexpressing K18R90C had lowest insulin count per unit area. The result is represented as the mean of the insulin vesicle count per unit area of the MIN6 cells. Here, the unit area represents cell area of 1μm^2. The highest number of insulin vesicle per unit area was found in control MIN6 cell and MIN6 cells overexpressing K8G62/K18WT. Higher insulin count per unit area was seen in control MIN6 cells compared to K8WT/K18WT and K8WT/K18R90C overexpressing MIN6. Statistical analysis was done using ten to thirteen cells for each comparative groups and significant difference was calculated with 2-tailed student's t-test where * = $p<0.05$, ** = $p<0.01$, *** = $p<0.001$ and **** = $p<0.0001$.

5.7 MIN6 cells overexpressing K8WT/K18WT are larger than untransfected MIN6 cells

The cell area of the MIN6 cells that overexpressed WT and mutant keratin were determined using Image J software and compared with each other. The results indicated that the MIN6 cells in the control group (untransfected MIN6 cells) had the smallest cell area while the WT overexpressing MIN6 cell were the largest ones (figure 18). Similarly, K8WT/K18WT overexpressing MIN6 cells had larger cell area compared to mutant keratin like K18R90C and KG62C overexpressing MIN6 cells (figure 18).The K-negative cells had the smallest

area due to absence of the keratin protein while the keratin expressing cells seems to have stretched out in terms of the boundary due to overexpression of the keratin filaments.

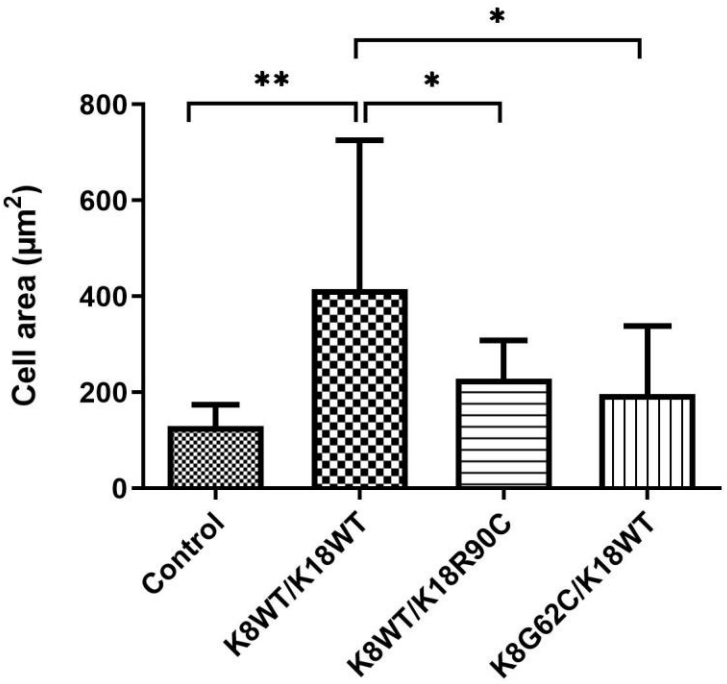

Figure 18. MIN6 cells overexpressing K8WT/K18WT were significantly larger in size than untransfected MIN6 cells and MIN6 cells overexpressing mutant keratins. The area of untransfected MIN6 cells was found to be lower than keratin overexpressing MIN6 cells and the comparison was significant with the MIN6 cells overexpressing K8WT/K18WT while similar comparison trend was seen with other groups. MIN6 cells overexpressing WT keratin filaments had significantly higher cell area compared to MIN6 cells overexpressing mutant strands of keratin (K8G62C and K18R90C). Statistical analysis was done using eleven to fifteen cells for each comparative groups and significant difference was calculated with 2-tailed student's t-test where * = $p<0.05$, ** = $p<0.01$ and *** = $p<0.001$.

5.8 During glucose stimulation of the MIN6 cells, the number of insulin vesicles decreased in keratin overexpressing cells

MIN6 cells were used for determining the effect of different levels of glucose in growth media and production of insulin vesicles per unit area. The MIN6 cells overexpressing K8/K18 had lower number of insulin vesicles compared to the untransfected keratin-free

MIN6 cells (control) (figure 19A) cultured in the normal media with glucose level of 25 mM which were incubated overnight.

During the experiment, the cells were treated with KRB buffer with different glucose concentrations. The cells were fixed using 1% PFA and stained for insulin, keratin and nuclei using immunofluorescence technique. Image processing was done using Image J and Bitplane Imaris using the spot counting feature after the confocal microscopy with Leica SP5 Matrix LSCM. From the result, it is found that the number of insulin vesicles is higher in untransfected MIN6 cells compared to WT keratin overexpressing MIN6 cells during stimulation by 5 mM glucose containing KRB solution for 5 minutes (figure 19). For higher durations and concentrations of glucose, there was no significant difference in number of insulin vesicle per unit cell area comparing keratin positive and keratin negative cell (figure 19B). However, a general trend was seen where untransfected MIN6 cells had higher number of insulin vesicles than the MIN6 cells overexpressing K8/K18 when incubated with same glucose concentration and time period.

A.

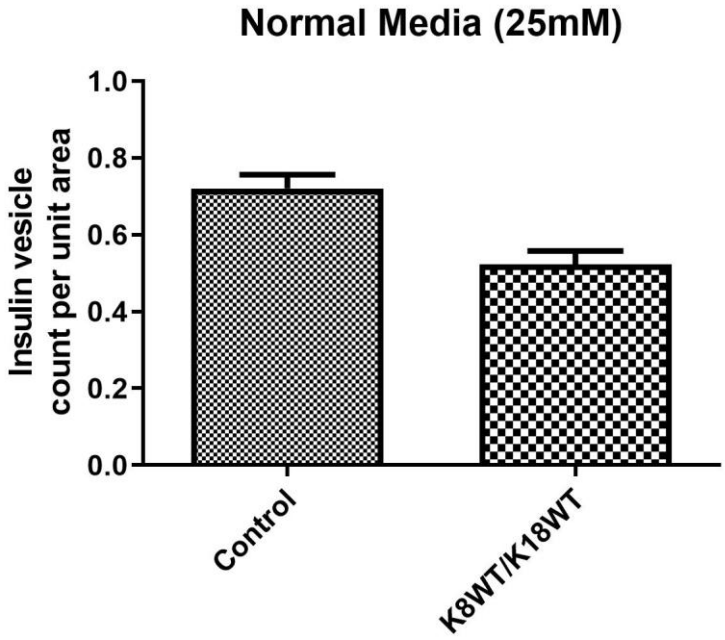

B.

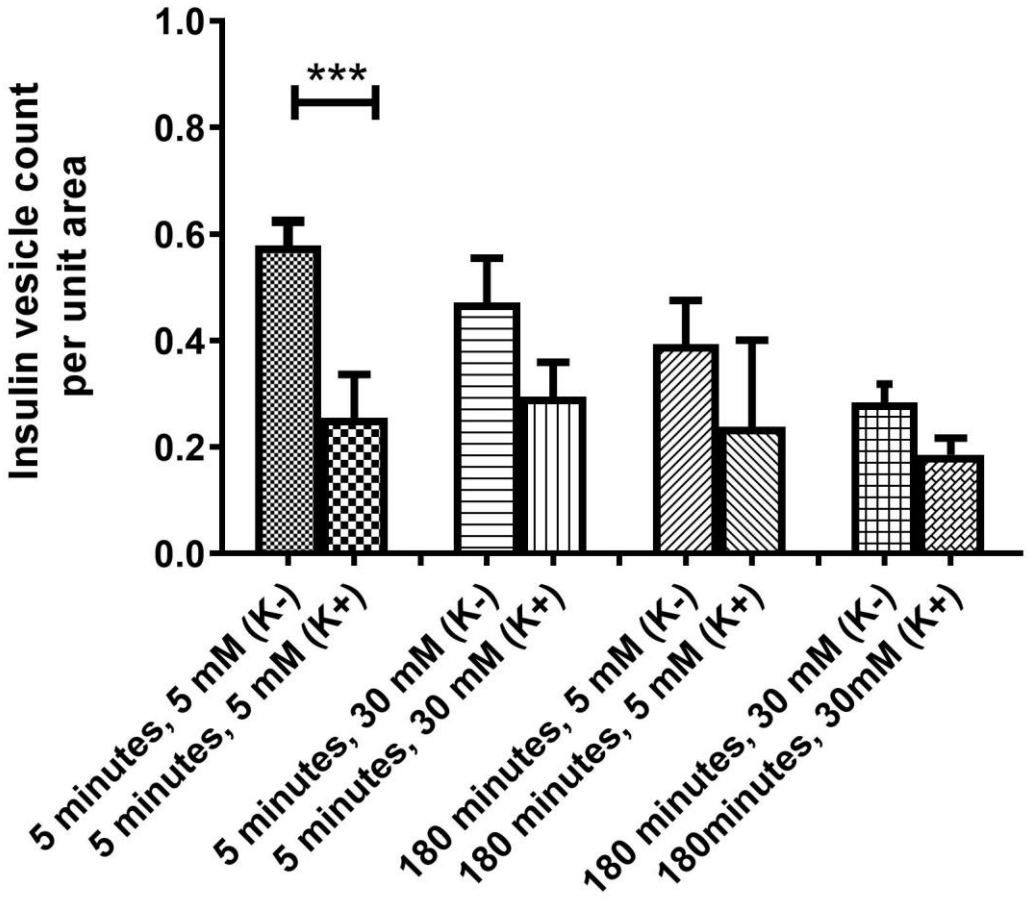

Figure 19. The number of insulin vesicles were not significantly higher in untransfected MIN6 cells and K8WT/K18WT overexpressing MIN6 cells except when treated with KRB buffer of 5mM glucose concentration. The results are represented as the mean of the insulin vesicle count per unit area of the MIN6 cells. Here, the unit area represents cell area of 1μm^2. (A) The number of insulin vesicles per unit area is significantly higher in control MIN6 cells which are almost keratin null compared to the K8WT/K18WT overexpressing MIN6 cells. (B) Different incubation time periods (5 minutes and 180 minutes) and different glucose concentrations (5 mM and 30 mM) were shown in the graph with a total of four study groups. Number of insulin vesicle per unit area was significantly higher in control MIN6 cells than K8WT/K18WT overexpressing MIN6 cells when incubated for 5 minutes at 5 mM glucose concentration. Similar trend was observed in all other study groups. For each group, nine to sixteen cells were considered for the statistical analysis. Statistical significance was calculated with 2-tailed Student's t-test where * = $p<0.05$, ** = $p<0.01$, *** = $p<0.001$ and **** = $p<0.0001$.

6 DISCUSSION

K8 and K18 are the major keratin types found in β-cells of pancreas. Since type I DM and type II DM are the one of the major diseases prevalent in modern world, it is important to understand the role of keratin in development of type I DM and type II DM by studying its influences on β-cells. Keratin IFs are known to be stress protector proteins and protect the cells during the time of mechanical, apoptotic, heat, oxidative and toxin related stresses in many types of cells in the body. Similarly, keratin intermediate filaments play a crucial role in mitochondrial morphology, dynamics and homeostasis in β-cells (Silvander et al., 2017). Insulin secretion is directly linked with the ATP generation in mitochondria in β-cells which suggests that mitochondrial activity has important role in insulin production (Jitrapakdee et al., 2010; Maechler, 2013). In this thesis work, the main goal was to find the role of keratin filaments in mitochondrial morphology and dynamics in the endocrine pancreatic cells. We observed the changes occurred in mitochondria and changes occurred in insulin secretion due to presence, absence or mutation of keratin filaments. In this study, MIN6 cells were used as substitute of the β-cells to run the planned experiments. MIN6 cells essentially are genetically modified β-cells but most importantly, they secretes insulin, which is a rare feature in pancreatic cell lines. However, MIN6 cells lacked keratin K8/K18 and transient transfection was required for overexpression of K8/K18. Other challenge was the transfection efficiency which was below 15% and the overexpression lasted only few days which prompted to perform the experiments as soon as they were transfected and enough K8/K18 were overexpressed by the cells (usually 2 days incubation after the transfection). This shortcoming of MIN6 cells, however, was advantageous in the sense that the untransfected cells served as keratin null cells and were used as control group for the experiments. Likewise another major advantage of using MIN6 cell line was that we were able to overexpress and perform experiments with mutated keratin filaments (K8G62C and K18R90C) which have their own importance as biomarkers in many diseases related to pancreas, liver, colon and skin (Ku et al., 2001; Omary, 2009; Owens et al., 2004). Various tests were performed with the wild type keratins as well as mutated keratin filaments and were compared side by side along with the keratin null untransfected MIN6 cells.

6.1 Presence of keratin filaments decreases the motility of mitochondria in MIN6 cells

We know that mitochondria are dynamic cell organelle and are constantly moving inside the cells (Silvander et al., 2017). One study in pancreatic acinar cells showed that the mitochondria strategically localized at specific positions in the cells to supply demanding ATP for various cellular functions like exocytotic secretions, activation or deactivation, Ca^{++} storage in ER and to protect nuclei by forming a barrier to block the Ca^{++} influx in the nucleus (Park et al., 2001). Cytoskeletal components like microfilaments, microtubules and few IFs are known to help the mitochondria in the transportation of the mitochondria in many types of cells (Ball and Singer, 1982; Drubin et al., 1993; Summerhayes et al., 1983; Yi et al., 2004). A study in mice showed that lack of motility of mitochondria due to deletion of kinesin motor protein (Kif1B) had fatal effect at the embryonic stage in the mice (Tanaka et al., 1998). Neurological disorders like Parkinsons disease, Alzheimer's disease and Huntington's disease are closely associated with defects in mitochondrial dynamics and morphology (Chen and Chan, 2009). Hence, it is essential to understand the mechanics of mitochondrial motility and the factors affecting it.

IFs have been known to affect the mitochondrial motility in cells. For instance, mitochondria in vimentin null cells have higher motility than normal cells with vimentin in fibroblast cells (Nekrasova et al., 2011). It has been previously studied that in $K8^{-/-}$ β-cells, the mitochondrial motility was increased compared to the $K8^{+/+}$ β-cells of mice (Silvander et al., 2017). In this thesis work, similar experiments using the MIN6 β-cell line were performed. The results in MIN6 cells was similar to the isolated β-cells where the keratin null WT MIN6 cells had higher mitochondrial motility while the MIN6 cells overexpressing K8/K18 had lesser mitochondrial motility by almost half the speed of mitochondria in WT MIN6 cells. It is possible that IFs like keratin and vimentin provide anchorage spots to mitochondria where they interact with these IFs with linker proteins like plectin1b and trichoplein (TCHP) (Matveeva et al., 2015; Toivola et al., 2005; Winter et al., 2008). K8 and K18 interact with mitochondrial fusion protein or mitofusin (MFN)2, through TCHP (Nishizawa et al., 2005; Silvander et al., 2017). It is possible that this interaction could provide the anchorage to the mitochondria which slowed the mitochondrial motility in K8/K18 overexpressing MIN6 cells. Since the levels of MFN2 is lower in $K8^{-/-}$ β-cells (Silvander et al., 2017) which correlates with the faster moving

mitochondria compared to K8 $^{+/+}$ β-cells, it would be interesting to measure the levels of MFN2 in MIN6 cells as well in future to see the effect of levels of MFN2 in mitochondrial motility as a function of keratin levels (Silvander et al., 2017). For this analysis to be doable, increased transfection efficiency of MIN6 cells needs to be achieved. Likewise this linkage of keratin and mitochondria also brings the attention to the colocalization of mitochondria and keratin filaments.

6.2 Colocalization of keratin filaments and mitochondria

It is already known that IFs like vimentin colocalize with mitochondrial membrane proteins (Nekrasova et al., 2011) and hence, it is possible that other IFs, such as keratins, also behave the same way. From the previous experiment it was found that the presence of keratin caused decrease in mitochondrial motility in MIN6 cells suggesting a possible anchorage of special mitochondrial TOM sites (TOM20) with specific keratin sites. TOM20 is one of the most abundant and important protein in the outer membrane of mitochondria and was chosen for the colocalization test with keratin filament.

It is highly possible that mitochondria colocalize on the keratin filaments (K8/K18) which is causing the retardation of the mitochondria in β-cells as well as MIN6 cells (Silvander et al., 2017). It is also possible that the mitochondrial colocalization to K8/K18 have direct link to the varied levels of MFN2 and TCHP, needed for interaction with K8/K18 in mitochondria, in $K8^{+/+}$ β-cells and $K8^{-/-}$ β-cells (Silvander et al., 2017). In the study of isolated pancreatic β-cells, K8 $^{+/+}$ β-cells had higher MFN2 and TCHP levels, which resulted in retardation of the mitochondria (Silvander et al., 2017). There is, thus, a good probability that there is more interaction or colocalization of the mitochondria with K8/K18.

In this experiment, the results were inconclusive due to problems that occurs during the image analysis of the images. Image J with COLOC2 plugin was used for the calculation of PCC. However, the software would crash and freeze the computer very often. Hence, this method to analyze the 2D images from the confocal microscope was not ideal way to analyze protein colocalization tasks. Instead, newer methods like proximity ligation assay (PLA) could be used to determine the colocalization of the mitochondrial TOM20 and keratin filaments. Limitations, like the spatial resolution of the LSCM, which is around 200 nm, severely limits the potential to get proper images for the visualization of the

colocalized areas. Since the points of these colocalized areas are much smaller, we need more powerful higher resolution microscopes like STED, SIM and other super resolution microscopes for the proper visualization of the colocalization through images. Although the actual colocalization of the keratin and TOM20 protein remains unclear from this experiment, there were certain 'hotspots' in the integrated images of the keratin (magenta) and TOM20 (green) which appeared grey (figure 13A), which would represent the colocalized points between keratin and TOM20. Hence, further study is needed to draw a clear conclusion. Likewise, more tests to find the protein levels of TOM20, MFN2 and TCHP would shed more light in this subject matter.

6.3 Presence or mutation of K8 and K18 influences the mitochondrial fusion and fragmentation

Mitochondrial fusion and fragmentation are one of the most important dynamic properties of mitochondria and are known to have significant impact on the metabolic activities like oxidative phosphorylation (OXPHOS) and Krebs cycle which helps in production of ATP in mitochondria. Mutations and change in levels of mitochondrial fusion proteins like MFN1, MFN2 and optic atrophy 1 (OPA1) causes altered levels of mitochondrial DNA (mtDNA) and dysfunctional OXPHOS process (Hermann et al., 1998; Mishra and Chan, 2016). Disease like Charcot-Marie-Tooth type 2A and dominant optic atrophy are related to mutation of these fusion proteins (Alexander et al., 2000, 1; Mishra and Chan, 2016; Züchner et al., 2004). Loss of MFN1 or MFN2 decreases the levels of mtDNA which results in reduction of respiratory chain functions and production of ATP in both cultured cells and mouse tissues (Chen et al., 2005; Mishra and Chan, 2016). Since loss of keratin filaments in $K8^{-/-}$ β-cells resulted in decreased MFN2 levels, it is highly relevant to investigate the mitochondrial fragmentation in MIN6 cells as well (Silvander et al., 2017).

Loss of keratin filament K8 in pancreatic β-cells of mouse leads to higher level of fragmentation of the mitochondria leading to smaller and rounder mitochondria compared to more cylindrical and elongated mitochondria in the normal β-cells (Silvander et al., 2017). In this thesis work, similar pattern of results were discovered where mitochondrial fragmentation was found highest in the keratin null untransfected MIN6 cells compared to the MIN6 cells overexpressing WT K8/K18 and K8/K18R90C. In isolated $K8^{-/-}$ β-cells it was found that the levels of mitochondrial fusion protein MFN2 was 25% lower than $K8^{+/+}$

β-cells which suggest that the mitochondrial structure is more fragmented in $K8^{-/-}$ β-cells than $K8^{+/+}$ β-cells (Silvander et al., 2017). In this study could be hypothesized that the MFN2 level in WT MIN6 is lower which results in more fragmented appearance of mitochondria. From the results, the mitochondria in the WT MIN6 cells were most fragmented followed MIN6 cells overexpressing K8WT/K18WT and K8WT/K18R90C, which had the least fragmentation score. This might be due to higher levels of MFN2 in keratin overexpressing MIN6 cells. The MIN6 cells overexpressing K18R90C had the lowest fragmentation score which predicts higher level of MFN2 in mitochondria. Since K18R90C is a severe kind of mutation which causes disruption of the filamentous structure of keratin (Ku et al., 2001), (figure 6b), the mitochondria may react abnormally under these condition. Similarly, since the increased fragmentation of the mitochondria is related to decreased cellular ATP production in many types of cell (Jheng et al., 2012; Rossignol et al., 2004), WT MIN6 cells might have decreased mitochondrial potential compared to keratin overexpressing MIN6 cells. With these findings, we can conclude that the presence of keratin filaments in MIN6 cells may cause less fragmentation of mitochondria.

6.4 Presence of WT K8/K18 increase the mitochondrial count in MIN6 cells

Generally eukaryotic cells have a wide range of per-cell mitochondria numbers ranging from 80 to 2000 (Cole, 2016) and these numbers are constantly changing due to frequent fission and fusion of mitochondria (Cole, 2016; Kowald and Kirkwood, 2011). The number of mitochondria varies with the types of cells and tissues and their functionalities. For instances, in plants, the green leaves, which requires high amount of energy for photosynthesis, have more mitochondria per-cell than the stem or woody tissues (Cole, 2016). In animals, similar trend is found where different mitochondrial count is found in organs like heart, liver, muscles and brain (Cole, 2016; Veltri et al., 1990).

In this thesis work, we tried to find effect of presence or absence or mutation of K8 and K18 on the number of mitochondria in the pancreatic cell line, MIN6 cells. Interestingly, there were different mitochondrial count in different groups of MIN6 cells test groups. During the image analysis procedure, it was found that some of cells were bigger in area while others were small, which can bias the result if we compare mitochondrial count per cell. So, to avoid this biasness, mitochondrial count per $1\mu m^2$ cell area were calculated and

represented in the results. First of all, comparing the WT MIN6 cells and MIN6 cells overexpressing WT K8/K18, it was found that the MIN6 cells overexpressing WT K8/K18 had significantly higher number of mitochondria. This suggest the possibility of K8/K18 helping the MIN6 cells in being more active regarding cellular functions like production of insulin and other pancreatic hormones and enzymes.

However, while the overexpression of WT K8/K18 resulted in higher numbers of mitochondria, a severe mutation that cause disruption of keratin filament at K18R90C had cancelling effect in terms of mitochondrial number i.e. the number of mitochondria in K18R90C is almost equal to number of mitochondria in nearly keratin null WT MIN6 cells. Hence, we can assume that the proper keratin filament structure is essential in proper functionality of the keratin filaments and these type of mutations severely hampers the normal functioning of keratin filament. It is also predicts that there is lower $\Delta\Psi m$ and insulin production in K18R90C overexpressing MIN6 cells than K18WT overexpressing MIN6 cells. Likewise, from this experiment, the number of mitochondria in K18R90C correlates to the result on the fragmentation level of mitochondria, where the group with K18R90C scored the lowest fragmentation level with highly clumped up mitochondrial morphology. All in all, we can see that K18R90C mutation has negative effect in the normal keratin functions.

Another mutation, K8G62C also had negative effect on the mitochondrial count. The mitochondrial count on MIN6 cells overexpressing K8G62C is similar to nearly keratin null normal untransfected MIN6 cells. Hence, we can summarize that while the overexpression of WT K8/K18 helped in increase the mitochondrial number in MIN6 cells, implying greater cellular activities, while the mutations like K18R90C and K8G62C had neutralized the effect of keratin on the mitochondrial count in the MIN6 cells where number of mitochondria is similar to the WT MIN6 cells.

6.5 Varying levels of keratin IF in MIN6 cells do not affect the ΔΨm in MIN6 cells

In isolated β-cells, the $\Delta\Psi m$ was found to be about half in the $K8^{-/-}$ β-cells compared to $K8^{+/+}$ beta cells and the ATP production was decreased to 44% which suggests that

presence of keratin filament increases the mitochondrial activities (Silvander et al., 2017). In this thesis work, we tried to find the effect of different levels of overexpression of K8/K18 on ΔΨm using MIN6 cells i.e. whether higher overexpression of K8/K18 would produce higher ΔΨm in the MIN6 cells or else. From this study, it was found that the higher or lower density of keratin filaments have little effect on the ΔΨm. The term 'higher keratin level' and 'lower keratin level' were separated by a median line that separated these two groups on the basis of their CTCF values and similar process was done for ΔΨm values. Taking these CTCF values from 28 MIN6 cells, it was found that there is no effect of level of overexpression of K8/K18 on ΔΨm.

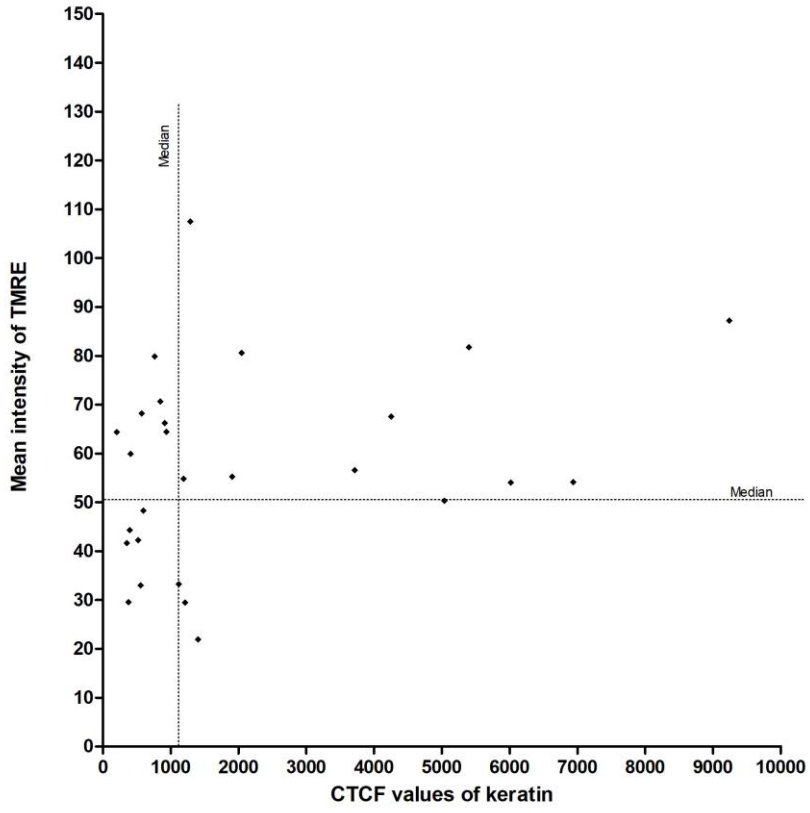

Figure 20. The hypothetical graph where the median line for the Y-axis (mean intensity of TMRE) is shifted from 54.62 to 50.34. This new assumption helps to support the argument that higher keratin levels in MIN6 cells leads to higher ΔΨm.

However, a slight shift on the median of mean intensity of TMRE from 54 to 50 can result in significant increase in number of cases with high keratin levels and high TMRE intensity in figure 15. We can see from the new hypothetical graph (figure 20) that the presence of higher level of keratin can actually result in higher level of ΔΨm. It also correlates to the

previous findings from β-cells where the absence of keratin in $K8^{-/-}$ β-cells resulted in lower ΔΨM compared to ΔΨM of $K8^{+/+}$ β-cells. Here, the inner membrane protein like cytochrome c level was decreased by 50% in $K8^{-/-}$ β-cells (Silvander et al., 2017). Similarly, $K8^{-/-}$ β-cells had less electron dense mitochondria compared to $K8^{+/+}$ β-cells which further suggest that there is less electro potential between the membranes of the mitochondria (Silvander et al., 2017). Since the number of cells used in this experiment was quite low, in future, higher number of cells should be tested to conclude if the higher level of keratin results in higher ΔΨm in MIN6 cells.

6.6 Overexpression of WT keratin filaments stretches the MIN6 cells

Normal untransfected MIN6 cells produce keratin filaments in negligible quantities and almost devoid of them. When MIN6 cells are transfected using electroporation methods to overexpress keratin filaments like K8WT/K18WT, K8WTK18R90C and K8G62C/K18WT, the area of the MIN6 cells increased significantly. The increment in the cell area might be due to the 'stretching' or 'swelling' effect of the overexpression of the keratin filaments which were previously not present inside the cells. MIN6 cells overexpressing WT keratins had higher area compared to both control and mutant keratin overexpressing groups. The significant difference in area between the WT keratin overexpressing and mutant keratin overexpressing MIN6 cells predict that the mutant keratin filaments, which had smaller area, do not have the proper mechanical strength to provide the mechanical 'stretch' that WT keratins provide to increase the cell area. As we know that K18R90C forms disruptive keratin filaments and hence will not provide enough mechanical force to stretch the MIN6 cells like WT variant. Similarly, K8G62 also being a mutant variant might not have the required mechanical force to stretch the MIN6 cells. Hence, further investigation on the mechanical roles of the mutant variants of keratin filaments would be interesting.

6.7 Overexpression of WT keratin filaments yielded higher number of mitochondria in MIN6 cells

In a study it was found that the average fasting blood glucose level was lower in $K8^{-/-}$ mice compared to $K8^{+/+}$ mice although the basal insulin levels for both cases were same (Alam et al., 2013). In this thesis work, I performed the comparative analysis of number of insulin vesicle in the MIN6 cell overexpressing WT and mutated keratin filaments with WT MIN6

cells. I found that the number of insulin vesicles in the MIN6 cells is variable in MIN6 cells overexpressing different types of keratin filaments. The number of insulin vesicles in WT MIN6 cells was significantly higher compared to MIN6 cells overexpressing WT K8/K18 and K18R90C keratin filaments. This result is opposite of what was found in case of $K8^{-/-}$ β-cells (Alam et al., 2013). The possible reason for this behavior in MIN6 cells might be that although the number of insulin vesicles is quite high in WT MIN6 cells, they might not be as active as they should be in terms of release of them into the blood stream when glucose is given as stimulant. It was observed in the study on β-cells that $K8^{-/-}$ β-cells had lower glucose sensitivity regarding the insulin level in the blood serum (Alam et al., 2013). It might suggest that although the normal untransfected MIN6 cells have higher number of insulin vesicles, they are not released to the blood stream which brings the attention to the exocytosis of the insulin vesicles and mechanism behind it. Similarly we should also consider the fact that MIN6 cells are mouse insulinoma cells and are genetically modified versions of β-cells. Likewise, MIN6 cells are among the very few cell lines that produces insulin. So, the actual production of insulin vesicles and the amount of insulin in MIN6 cells may not correlate with the normal β-cells themselves. Further investigation and direct comparisons of insulin productions in β-cells and MIN6 cells would be interesting for future tests.

The result in MIN6 cells overexpressing mutated K18R90C also showed lower insulin vesicle count compared to the WT MIN6 cells. However, MIN6 cells overexpressing K8G62C had similar number of insulin vesicle as WT MIN6 cells. We have seen from the previous results in this thesis work that mutations in these keratin proteins have yielded abnormal results. Separate detailed studies on these mutations on keratin types are needed in future for more confirmatory and reliable results.

6.8 Overexpression of keratin filaments helps in higher number of insulin vesicle production in MIN6 cells

MIN6 cells are one of the few pancreatic cell lines that produce insulin like β-cells although they are cancerous cells. β-cells are highly sensitive to change in glucose concentration in the surrounding physiological environment and similar insulin sensitivity is shown by MIN6 cells (Ishihara et al., 1993). In this thesis work, when these MIN6 cells were incubated at normal incubation condition with DMEM media with 25 mM glucose

concentration, it was found that the WT MIN6 cells had significantly higher number of insulin vesicles compared to WT K8/K18 overexpressing MIN6 cells. This result is consistent with the previous experiment where WT MIN6 cells were producing higher number of insulin vesicles than WT K8/K18 overexpressing MIN6 cells (figure 17). However, it does not agrees to the findings from the study done on β-cells (Alam et al., 2013).

Similarly, I compared the number of insulin vesicles produced in WT MIN6 cells and WT K8/K18 overexpressing MIN6 cells with two different glucose stimulation concentrations (5 mM and 30 mM) in the incubation media at two different incubation time points (5 minutes and 180 minutes), creating four case groups. In previous studies on MIN6 cells, the minimum glucose concentration used to stimulate the MIN6 cell insulin secretion was 5mM and the secretion level increased to seven fold at 25 mM and stayed there upto 50 mM (Ishihara et al., 1993), hence 5 mM and 30 mM glucose for stimulation of insulin vesicles were chosen in this experiment. Again in this experiment, it was found that the number of insulin vesicles was higher in WT MIN6 cells when grown in normal media at 25 mM glucose. Similarly, when the cells were incubated in different glucose concentration (5 mM and 30 mM) and incubated for different time periods (5 and 180 minutes), a similar trend of insulin vesicle counts were observed. The number of insulin vesicles was in all my studies always greater in WT MIN6 cells that are almost devoid of the keratin filament compared to the MIN6 cells overexpressing the keratin filaments (K8WT/K18WT).

There is significant difference in number of insulin vesicle in the cells when they were incubated for 5 minutes at 5 mM glucose concentration. In other cases, the longer we incubated the cell in the KRB buffer solution, lesser the difference in number of insulin vesicles were found. However, this indicates that the WT MIN6 cells had higher number of insulin vesicles. It can be deduced that the normal functionality of the MIN6 cells might have died due to the incubation in KRB buffer solution rather than the normal growth media. Nonetheless, it was clearly seen that the incubation for 5 minutes at 5 mM glucose concentration have significant difference in insulin vesicle numbers in WT MIN6 cells and K8/K18 overexpressing MIN6 cells. We can also see that the increase of glucose concentration from 5 mM to 30 mM while incubating for same 5 minutes resulted in decline in insulin vesicle production in normal MIN6 cells while it remained similar level

in keratin overexpressing MIN6 cell and this trend is evident in other cases as well. So, we can deduce that overexpression of keratin filament may have 'desensitized' the glucose response of the MIN6 cells and the production of insulin vesicle remains less effected while there is sharp decline in insulin production in WT MIN6 cells that are almost devoid of the keratin filaments. However, since there was increase in insulin production from 5 to 30mM glucose concentration, human errors might have occurred and it would be wise to repeat the experiment once again.

7 CONCLUSION

In conclusion, presence or absence of keratin IFs (K8WT/K18WT) and mutation of these keratins (K8G62C and K18R90C) have significant impact on the mitochondrial motility, mitochondrial fragmentation, ΔΨm and mitochondrial count. The changes on mitochondrial morphology and dynamics is related with the changes in insulin production in the MIN6 cells.

Table 5: Role of keratin IF in mitochondrial morphology, dynamics and insulin secretion in MIN6 cells. Keratin plays vital role in mitochondrial motility, fragmentation, membrane potential and insulin production in MIN6 cells.

	Untransfected MIN6 Cells	**K8WT/K18 WT**	**K8WT/K18 R90C**	**K8G62C/ K18WT**	**Discussion**
Mitochondrial motility	Higher	Lower	-	-	Higher mitochondrial motility in untransfected MIN6 cells
Mitochondria/ keratin colocalization	-	Not significant	Not significant	-	No significant colocalization between the keratin and mitochondria found
Mitochondrial fragmentation	Highest	Medium	Lowest	Highest	Untranfected MIN6 cells and MIN6 cells overexpressing K8G62C had highest level of mitochondrial fragmentation while MIN6 cells overexpressing K18R90C had lowest mitochondrial fragmentation.
Keratin levels vs. ΔΨm	Equal	Equal	-	-	There was no significant difference in ΔΨm due to varying levels of keratin in MIN6 cells.
Number of mitochondria per unit cell area	Low	High	Low		Number of mitochondria per unit cell area was significantly higher in K8WT/K18Wt overexpressing MIN6 cells
Number of insulin vesicles per unit cell area	High	Low	Low	High	Number of insulin vesicles per unit cell area is highest in untransfected MIN6 cells and MIN6 cells overexpressing K8G62C while low in K8WT/K18WT and K18R90C overexpressing MIN6 cells.
Cell size	Smallest	Largest	Small	Small	MIN6 cells that overexpressed K8WT/K18WT had largest cell size.
Insulin vesicle count per unit cell area at 25mM	Higher count	Lower count	-	-	Number of insulin vesicle is lower in K8WT/K18WT overexpressing MIN6 cells.

8 ACKNOWLEDGEMENTS

The experiments for this Master's thesis was performed in Diana Toivola's Lab in Biocity building, 2nd floor. I want to thank both University of Turku and Åbo Akademi University for providing working facilities in the Biocity building. I want to thank my supervisor, Diana Toivola for giving me the support and guidance needed to complete this study and letting me work for two years in the pancreas project. I would also like to thank my mentor Jonas Silvander for guiding me through all the steps of the planning and running experiments. I am thankful for Catharina Alam for her instructions and guidance during the thesis writing period. I am also very grateful for Angeli Kumari Ilieva and Terhi Helenius for giving me suggestions and helping me with the writing of this thesis. I am also thankful to Jari Korhonen and Jouko Sandholm for microscopy trainings. I am thankful to my parents, Tejlal Shrestha and Maya Laxmi Shrestha and my wife Aruna for all the support and inspiration each and every day. Finally, I am very grateful to Joel, Calle and all the lab members of Diana Toivola laboratory for all the support and help.

9 REFERENCES

Achtstätter, T., R. Moll, B. Moore, and W.W. Franke. 1985. Cytokeratin polypeptide patterns of different epithelia of the human male urogenital tract: immunofluorescence and gel electrophoretic studies. *J. Histochem. Cytochem. Off. J. Histochem. Soc.* 33:415–426. doi:10.1177/33.5.2580881.

Alam, C., J.S.G. Silvander, T.O. Helenius, and D.M. Toivola. 2018. Decreased levels of keratin 8 sensitizes mice to streptozotocin-induced diabetes. *Acta Physiol.*

Alam, C.M., J.S.G. Silvander, E.N. Daniel, G.-Z. Tao, S.M. Kvarnström, P. Alam, M.B. Omary, A. Hänninen, and D.M. Toivola. 2013. Keratin 8 modulates β-cell stress responses and normoglycaemia. *J. Cell Sci.* 126:5635–5644. doi:10.1242/jcs.132795.

Alberts, B., A. Johnson, J. Lewis, M. Raff, K. Roberts, and P. Walter. 2002a. The Self-Assembly and Dynamic Structure of Cytoskeletal Filaments.

Alberts, B., A. Johnson, J. Lewis, M. Raff, K. Roberts, and P. Walter. 2002b. The Mitochondrion.

Alexander, C., M. Votruba, U.E. Pesch, D.L. Thiselton, S. Mayer, A. Moore, M. Rodriguez, U. Kellner, B. Leo-Kottler, G. Auburger, S.S. Bhattacharya, and B. Wissinger. 2000. OPA1, encoding a dynamin-related GTPase, is mutated in autosomal dominant optic atrophy linked to chromosome 3q28. *Nat. Genet.* 26:211–215. doi:10.1038/79944.

Ball, E.H., and S.J. Singer. 1982. Mitochondria are associated with microtubules and not with intermediate filaments in cultured fibroblasts. *Proc. Natl. Acad. Sci. U. S. A.* 79:123–126.

Baribault, H., J. Penner, R.V. Iozzo, and M. Wilson-Heiner. 1994. Colorectal hyperplasia and inflammation in keratin 8-deficient FVB/N mice. *Genes Dev.* 8:2964–2973.

Baribault, H., J. Price, K. Miyai, and R.G. Oshima. 1993. Mid-gestational lethality in mice lacking keratin 8. *Genes Dev.* 7:1191–1202.

Bauer, C., and P. Traub. 1995. Interaction of intermediate filaments with ribosomes in vitro. *Eur. J. Cell Biol.* 68:288–296.

Bausewein, T., D.J. Mills, J.D. Langer, B. Nitschke, S. Nussberger, and W. Kühlbrandt. 2017. Cryo-EM Structure of the TOM Core Complex from Neurospora crassa. *Cell*. 170:693-700.e7. doi:10.1016/j.cell.2017.07.012.

Becker, L., M. Bannwarth, C. Meisinger, K. Hill, K. Model, T. Krimmer, R. Casadio, K.N. Truscott, G.E. Schulz, N. Pfanner, and R. Wagner. 2005. Preprotein translocase of the outer mitochondrial membrane: reconstituted Tom40 forms a characteristic TOM pore. *J. Mol. Biol.* 353:1011–1020. doi:10.1016/j.jmb.2005.09.019.

Bertelli, E., and M. Bendayan. 2005. Association between Endocrine Pancreas and Ductal System. More than an Epiphenomenon of Endocrine Differentiation and Development? *J. Histochem. Cytochem.* 53:1071–1086. doi:10.1369/jhc.5R6640.2005.

Beutner, E.H. 1961. IMMUNOFLUORESCENT STAINING: THE FLUORESCENT ANTIBODY METHOD1. *Bacteriol. Rev.* 25:49–76.

Block, J., V. Schroeder, P. Pawelzyk, N. Willenbacher, and S. Köster. 2015. Physical properties of cytoplasmic intermediate filaments. *Biochim. Biophys. Acta*. 1853:3053–3064. doi:10.1016/j.bbamcr.2015.05.009.

Block, R.J. 1951. Chemical Classification of Keratins. *Ann. N. Y. Acad. Sci.* 53:608–612. doi:10.1111/j.1749-6632.1951.tb31962.x.

Bonora, M., S. Patergnani, A. Rimessi, E. De Marchi, J.M. Suski, A. Bononi, C. Giorgi, S. Marchi, S. Missiroli, F. Poletti, M.R. Wieckowski, and P. Pinton. 2012. ATP synthesis and storage. *Purinergic Signal.* 8:343–357. doi:10.1007/s11302-012-9305-8.

Bousquet, O., L. Ma, S. Yamada, C. Gu, T. Idei, K. Takahashi, D. Wirtz, and P.A. Coulombe. 2001. The nonhelical tail domain of keratin 14 promotes filament bundling and enhances the mechanical properties of keratin intermediate filaments in vitro. *J. Cell Biol.* 155:747–754. doi:10.1083/jcb.200104063.

Bowden, P.E., R.A. Quinlan, D. Breitkreutz, and N.E. Fusenig. 1984. Proteolytic modification of acidic and basic keratins during terminal differentiation of mouse and human epidermis. *Eur. J. Biochem.* 142:29–36.

Bragulla, H.H., and D.G. Homberger. 2009. Structure and functions of keratin proteins in simple, stratified, keratinized and cornified epithelia. *J. Anat.* 214:516–559. doi:10.1111/j.1469-7580.2009.01066.x.

Cabrera, O., D.M. Berman, N.S. Kenyon, C. Ricordi, P.-O. Berggren, and A. Caicedo. 2006. The unique cytoarchitecture of human pancreatic islets has implications for islet cell function. *Proc. Natl. Acad. Sci. U. S. A.* 103:2334–2339. doi:10.1073/pnas.0510790103.

Cavestro, G.M., L. Frulloni, A. Nouvenne, T.M. Neri, B. Calore, B. Ferri, P. Bovo, L. Okolicsanyi, F. Di Mario, and G. Cavallini. 2003. Association of keratin 8 gene mutation with chronic pancreatitis. *Dig. Liver Dis. Off. J. Ital. Soc. Gastroenterol. Ital. Assoc. Study Liver*. 35:416–420.

Chacinska, A., C.M. Koehler, D. Milenkovic, T. Lithgow, and N. Pfanner. 2009. Importing mitochondrial proteins: machineries and mechanisms. *Cell*. 138:628–644. doi:10.1016/j.cell.2009.08.005.

Chamcheu, J.C., I.A. Siddiqui, D.N. Syed, V.M. Adhami, M. Liovic, and H. Mukhtar. 2011. Keratin Gene Mutations in Disorders of Human Skin and its Appendages. *Arch. Biochem. Biophys.* 508:123–137. doi:10.1016/j.abb.2010.12.019.

Chan, S.J., P. Keim, and D.F. Steiner. 1976. Cell-free synthesis of rat preproinsulins: characterization and partial amino acid sequence determination. *Proc. Natl. Acad. Sci. U. S. A.* 73:1964–1968.

Chang, L., K. Barlan, Y.-H. Chou, B. Grin, M. Lakonishok, A.S. Serpinskaya, D.K. Shumaker, H. Herrmann, V.I. Gelfand, and R.D. Goldman. 2009. The dynamic properties of intermediate filaments during organelle transport. *J. Cell Sci.* 122:2914–2923. doi:10.1242/jcs.046789.

Chen, H., and D.C. Chan. 2009. Mitochondrial dynamics–fusion, fission, movement, and mitophagy–in neurodegenerative diseases. *Hum. Mol. Genet.* 18:R169–R176. doi:10.1093/hmg/ddp326.

Chen, H., A. Chomyn, and D.C. Chan. 2005. Disruption of Fusion Results in Mitochondrial Heterogeneity and Dysfunction. *J. Biol. Chem.* 280:26185–26192. doi:10.1074/jbc.M503062200.

Chiang, J.L., M.S. Kirkman, L.M.B. Laffel, and A.L. Peters. 2014. Type 1 Diabetes Through the Life Span: A Position Statement of the American Diabetes Association. *Diabetes Care*. 37:2034–2054. doi:10.2337/dc14-1140.

Cole, L.W. 2016. The Evolution of Per-cell Organelle Number. *Front. Cell Dev. Biol.* 4. doi:10.3389/fcell.2016.00085.

Cooper, G.M. 2000. Mitochondria.

Coore, H.G., and P.J. Randle. 1964. Regulation of insulin secretion studied with pieces of rabbit pancreas incubated in vitro. *Biochem. J.* 93:66–78.

Coulombe, P.A., R. Kopan, and E. Fuchs. 1989. Expression of keratin K14 in the epidermis and hair follicle: insights into complex programs of differentiation. *J. Cell Biol.* 109:2295–2312.

Coulombe, P.A., and M.B. Omary. 2002. "Hard" and "soft" principles defining the structure, function and regulation of keratin intermediate filaments. *Curr. Opin. Cell Biol.* 14:110–122.

Coulombe, P.A., X. Tong, S. Mazzalupo, Z. Wang, and P. Wong. 2004. Great promises yet to be fulfilled: defining keratin intermediate filament function in vivo. *Eur. J. Cell Biol.* 83:735–746. doi:10.1078/0171-9335-00443.

Coulombe, P.A., M. Wawersik, R.D. Paladini, and E. Noensie. 1998. Type I keratin 16 forms relatively unstable tetrameric assembly subunits with various type II keratin partners: biochemical basis and functional implications. *Biol. Bull.* 194:364–365; discussion 365-366. doi:10.2307/1543114.

Dale, B.A., K.A. Holbrook, J.R. Kimball, M. Hoff, and T.T. Sun. 1985. Expression of epidermal keratins and filaggrin during human fetal skin development. *J. Cell Biol.* 101:1257–1269.

Danielsson, A., F. Pontén, L. Fagerberg, B.M. Hallström, J.M. Schwenk, M. Uhlén, O. Korsgren, and C. Lindskog. 2014. The Human Pancreas Proteome Defined by Transcriptomics and Antibody-Based Profiling. *PLoS ONE*. 9. doi:10.1371/journal.pone.0115421.

Dean, P.M. 1973. Ultrastructural morphometry of the pancreatic -cell. *Diabetologia*. 9:115–119.

Debus, E., K. Weber, and M. Osborn. 1982. Monoclonal cytokeratin antibodies that distinguish simple from stratified squamous epithelia: characterization on human tissues. *EMBO J.* 1:1641–1647.

Dolenšek, J., M.S. Rupnik, and A. Stožer. 2015. Structural similarities and differences between the human and the mouse pancreas. *Islets*. 7. doi:10.1080/19382014.2015.1024405.

Drubin, D.G., H.D. Jones, and K.F. Wertman. 1993. Actin structure and function: roles in mitochondrial organization and morphogenesis in budding yeast and identification of the phalloidin-binding site. *Mol. Biol. Cell*. 4:1277–1294.

Dubois, P.M. 1999. The Exocrine and Endocrine Pancreas: Embryology and Histology. *In* Radiology of the Pancreas. A.L. Baert, G. Delorme, and L. Van Hoe, editors. Springer Berlin Heidelberg, Berlin, Heidelberg. 1–8.

Dunn, M.F. 2005. Zinc–Ligand Interactions Modulate Assembly and Stability of the Insulin Hexamer – A Review. *Biometals*. 18:295–303. doi:10.1007/s10534-005-3685-y.

Eckert, R.L. 1988. Sequence of the human 40-kDa keratin reveals an unusual structure with very high sequence identity to the corresponding bovine keratin. *Proc. Natl. Acad. Sci. U. S. A.* 85:1114–1118.

Efrat, S., and D. Hanahan. 1987. Bidirectional activity of the rat insulin II 5'-flanking region in transgenic mice. *Mol. Cell. Biol.* 7:192–198.

Eichner, R., T.T. Sun, and U. Aebi. 1986. The role of keratin subfamilies and keratin pairs in the formation of human epidermal intermediate filaments. *J. Cell Biol.* 102:1767–1777.

Er Rafik, M., J. Doucet, and F. Briki. 2004. The intermediate filament architecture as determined by X-ray diffraction modeling of hard alpha-keratin. *Biophys. J.* 86:3893–3904. doi:10.1529/biophysj.103.034694.

Fradette, J., L. Germain, P. Seshaiah, and P.A. Coulombe. 1998. The type I keratin 19 possesses distinct and context-dependent assembly properties. *J. Biol. Chem.* 273:35176–35184.

Freshney, R.I. 2005. Culture of Animal Cells: A Manual of Basic Technique. Wiley-Liss, Hoboken, NJ, USA. 642 pp.

Fu, Z., E.R. Gilbert, and D. Liu. 2013. Regulation of Insulin Synthesis and Secretion and Pancreatic Beta-Cell Dysfunction in Diabetes. *Curr. Diabetes Rev.* 9:25–53.

Gauthier, B.R., and C.B. Wollheim. 2008. Synaptotagmins bind calcium to release insulin. *Am. J. Physiol. Endocrinol. Metab.* 295:E1279-1286. doi:10.1152/ajpendo.90568.2008.

Gilbert, S., A. Loranger, and N. Marceau. 2004. Keratins Modulate c-Flip/Extracellular Signal-Regulated Kinase 1 and 2 Antiapoptotic Signaling in Simple Epithelial Cells. *Mol. Cell. Biol.* 24:7072–7081. doi:10.1128/MCB.24.16.7072-7081.2004.

Gu, L.-H., and P.A. Coulombe. 2005. Defining the properties of the nonhelical tail domain in type II keratin 5: insight from a bullous disease-causing mutation. *Mol. Biol. Cell*. 16:1427–1438. doi:10.1091/mbc.E04-06-0498.

Guo, Y., and Y. Zheng. 2015. Lamins position the nuclear pores and centrosomes by modulating dynein. *Mol. Biol. Cell*. 26:3379–3389. doi:10.1091/mbc.E15-07-0482.

Habtezion, A., D.M. Toivola, E.C. Butcher, and M.B. Omary. 2005. Keratin-8-deficient mice develop chronic spontaneous Th2 colitis amenable to antibiotic treatment. *J. Cell Sci.* 118:1971–1980. doi:10.1242/jcs.02316.

Hanukoglu, I., and E. Fuchs. 1983a. The cDNA sequence of a Type II cytoskeletal keratin reveals constant and variable structural domains among keratins. *Cell*. 33:915–924.

Hanukoglu, I., and E. Fuchs. 1983b. The cDNA sequence of a Type II cytoskeletal keratin reveals constant and variable structural domains among keratins. *Cell*. 33:915–924.

Hatzfeld, M., and M. Burba. 1994. Function of type I and type II keratin head domains: their role in dimer, tetramer and filament formation. *J. Cell Sci.* 107 (Pt 7):1959–1972.

Held, N.M., and R.H. Houtkooper. 2015. Mitochondrial quality control pathways as determinants of metabolic health. *Bioessays*. 37:867–876. doi:10.1002/bies.201500013.

Henquin, J.C. 2009. Regulation of insulin secretion: a matter of phase control and amplitude modulation. *Diabetologia*. 52:739–751. doi:10.1007/s00125-009-1314-y.

Henry, B.M., B. Skinningsrud, K. Saganiak, P.A. Pękala, J.A. Walocha, and K.A. Tomaszewski. 2019. Development of the human pancreas and its vasculature — An integrated review covering anatomical, embryological, histological, and molecular aspects. *Ann. Anat. - Anat. Anz.* 221:115–124. doi:10.1016/j.aanat.2018.09.008.

Hermann, G.J., J.W. Thatcher, J.P. Mills, K.G. Hales, M.T. Fuller, J. Nunnari, and J.M. Shaw. 1998. Mitochondrial Fusion in Yeast Requires the Transmembrane GTPase Fzo1p. *J. Cell Biol.* 143:359–373. doi:10.1083/jcb.143.2.359.

Hernandez, B.Y., H.F. Frierson, C.A. Moskaluk, Y.J. Li, L. Clegg, T.R. Cote, M.E. McCusker, B.F. Hankey, B.K. Edwards, and M.T. Goodman. 2005. CK20 and CK7 protein expression in colorectal cancer: demonstration of the utility of a population-based tissue microarray. *Hum. Pathol.* 36:275–281. doi:10.1016/j.humpath.2005.01.013.

Herrmann, H., and U. Aebi. 2004. Intermediate filaments: molecular structure, assembly mechanism, and integration into functionally distinct intracellular Scaffolds. *Annu. Rev. Biochem.* 73:749–789. doi:10.1146/annurev.biochem.73.011303.073823.

Herrmann, H., S.V. Strelkov, P. Burkhard, and U. Aebi. 2009. Intermediate filaments: primary determinants of cell architecture and plasticity. *J. Clin. Invest.* 119:1772–1783. doi:10.1172/JCI38214.

Herrmann, H., S.V. Strelkov, B. Feja, K.R. Rogers, M. Brettel, A. Lustig, M. Häner, D.A. Parry, P.M. Steinert, P. Burkhard, and U. Aebi. 2000. The intermediate filament protein consensus motif of helix 2B: its atomic structure and contribution to assembly. *J. Mol. Biol.* 298:817–832. doi:10.1006/jmbi.2000.3719.

Hesse, M., T.M. Magin, and K. Weber. 2001. Genes for intermediate filament proteins and the draft sequence of the human genome: novel keratin genes and a surprisingly high number of pseudogenes related to keratin genes 8 and 18. *J. Cell Sci.* 114:2569–2575.

Hill, K., K. Model, M.T. Ryan, K. Dietmeier, F. Martin, R. Wagner, and N. Pfanner. 1998. Tom40 forms the hydrophilic channel of the mitochondrial import pore for preproteins [see comment]. *Nature*. 395:516–521. doi:10.1038/26780.

Hoogenraad, N.J., L.A. Ward, and M.T. Ryan. 2002. Import and assembly of proteins into mitochondria of mammalian cells. *Biochim. Biophys. Acta*. 1592:97–105.

Hutton, E., R.D. Paladini, Q.C. Yu, M. Yen, P.A. Coulombe, and E. Fuchs. 1998. Functional differences between keratins of stratified and simple epithelia. *J. Cell Biol.* 143:487–499.

Irvine, A.D., L.D. Corden, O. Swensson, B. Swensson, J.E. Moore, D.G. Frazer, F.J. Smith, R.G. Knowlton, E. Christophers, R. Rochels, J. Uitto, and W.H. McLean. 1997. Mutations in cornea-specific keratin K3 or K12 genes cause Meesmann's corneal dystrophy. *Nat. Genet.* 16:184–187. doi:10.1038/ng0697-184.

Ishihara, H., T. Asano, K. Tsukuda, H. Katagiri, K. Inukai, M. Anai, M. Kikuchi, Y. Yazaki, J.I. Miyazaki, and Y. Oka. 1993. Pancreatic beta cell line MIN6 exhibits characteristics of glucose metabolism and glucose-stimulated insulin secretion similar to those of normal islets. *Diabetologia*. 36:1139–1145.

Jheng, H.-F., P.-J. Tsai, S.-M. Guo, L.-H. Kuo, C.-S. Chang, I.-J. Su, C.-R. Chang, and Y.-S. Tsai. 2012. Mitochondrial fission contributes to mitochondrial dysfunction and insulin resistance in skeletal muscle. *Mol. Cell. Biol.* 32:309–319. doi:10.1128/MCB.05603-11.

Jitrapakdee, S., A. Wutthisathapornchai, J.C. Wallace, and M.J. MacDonald. 2010. Regulation of insulin secretion: role of mitochondrial signalling. *Diabetologia*. 53:1019–1032. doi:10.1007/s00125-010-1685-0.

Karantza, V. 2011. Keratins in health and cancer: more than mere epithelial cell markers. *Oncogene*. 30:127–138. doi:10.1038/onc.2010.456.

Kazerounian, S., J. Uitto, and S. Aho. 2002. Unique role for the periplakin tail in intermediate filament association: specific binding to keratin 8 and vimentin. *Exp. Dermatol.* 11:428–438.

Kim, A., K. Miller, J. Jo, G. Kilimnik, P. Wojcik, and M. Hara. 2009. Islet architecture. *Islets*. 1:129–136. doi:10.4161/isl.1.2.9480.

Kim, S., P. Wong, and P.A. Coulombe. 2006. A keratin cytoskeletal protein regulates protein synthesis and epithelial cell growth. *Nature*. 441:362–365. doi:10.1038/nature04659.

Kowald, A., and T.B.L. Kirkwood. 2011. Evolution of the mitochondrial fusion-fission cycle and its role in aging. *Proc. Natl. Acad. Sci. U. S. A.* 108:10237–10242. doi:10.1073/pnas.1101604108.

Ku, N.O., R. Gish, T.L. Wright, and M.B. Omary. 2001. Keratin 8 mutations in patients with cryptogenic liver disease. *N. Engl. J. Med.* 344:1580–1587. doi:10.1056/NEJM200105243442103.

Ku, N.-O., J.K. Lim, S.M. Krams, C.O. Esquivel, E.B. Keeffe, T.L. Wright, D.A.D. Parry, and M.B. Omary. 2005. Keratins as susceptibility genes for end-stage liver disease. *Gastroenterology*. 129:885–893. doi:10.1053/j.gastro.2005.06.065.

Ku, N.O., S. Michie, R.G. Oshima, and M.B. Omary. 1995. Chronic hepatitis, hepatocyte fragility, and increased soluble phosphoglycokeratins in transgenic mice expressing a keratin 18 conserved arginine mutant. *J. Cell Biol.* 131:1303–1314. doi:10.1083/jcb.131.5.1303.

Ku, N.-O., and M.B. Omary. 2006. A disease- and phosphorylation-related nonmechanical function for keratin 8. *J. Cell Biol.* 174:115–125. doi:10.1083/jcb.200602146.

Ku, N.O., X. Zhou, D.M. Toivola, and M.B. Omary. 1999. The cytoskeleton of digestive epithelia in health and disease. *Am. J. Physiol.* 277:G1108-1137. doi:10.1152/ajpgi.1999.277.6.G1108.

Kulkarni, R.N. 2004. The islet β-cell. *Int. J. Biochem. Cell Biol.* 36:365–371. doi:10.1016/j.biocel.2003.08.010.

Kumemura, H., M. Harada, M.B. Omary, S. Sakisaka, T. Suganuma, M. Namba, and M. Sata. 2004. Aggregation and loss of cytokeratin filament networks inhibit golgi organization in liver-derived epithelial cell lines. *Cell Motil. Cytoskeleton*. 57:37–52. doi:10.1002/cm.10152.

Kumemura, H., M. Harada, C. Yanagimoto, H. Koga, T. Kawaguchi, S. Hanada, E. Taniguchi, T. Ueno, and M. Sata. 2008. Mutation in keratin 18 induces mitochondrial fragmentation in liver-derived epithelial cells. *Biochem. Biophys. Res. Commun.* 367:33–40. doi:10.1016/j.bbrc.2007.12.116.

Lang, J. 1999. Molecular mechanisms and regulation of insulin exocytosis as a paradigm of endocrine secretion. *Eur. J. Biochem.* 259:3–17.

Langbein, L., M.A. Rogers, H. Winter, S. Praetzel, U. Beckhaus, H.R. Rackwitz, and J. Schweizer. 1999. The catalog of human hair keratins. I. Expression of the nine type I members in the hair follicle. *J. Biol. Chem.* 274:19874–19884.

Lodish, H., A. Berk, S.L. Zipursky, P. Matsudaira, D. Baltimore, and J. Darnell. 2000a. The Dynamic Cell.

Lodish, H., A. Berk, S.L. Zipursky, P. Matsudaira, D. Baltimore, and J. Darnell. 2000b. Intermediate Filaments.

Ma, L., S. Yamada, D. Wirtz, and P.A. Coulombe. 2001. A “hot-spot” mutation alters the mechanical properties of keratin filament networks. *Nat. Cell Biol.* 3:503–506. doi:10.1038/35074576.

Maechler, P. 2013. Mitochondrial function and insulin secretion. *Mol. Cell. Endocrinol.* 379:12–18. doi:10.1016/j.mce.2013.06.019.

Martínez-Reyes, I., L.P. Diebold, H. Kong, M. Schieber, H. Huang, C.T. Hensley, M.M. Mehta, T. Wang, J.H. Santos, R. Woychik, E. Dufour, J.N. Spelbrink, S.E. Weinberg, Y. Zhao, R.J. DeBerardinis, and N.S. Chandel. 2016. TCA cycle and mitochondrial membrane potential are necessary for diverse biological functions. *Mol. Cell*. 61:199–209. doi:10.1016/j.molcel.2015.12.002.

Matsumo. 2003. Cell Biological Applications of Confocal Microscopy. Academic Press. 521 pp.

Matveeva, E.A., L.S. Venkova, I.S. Chernoivanenko, and A.A. Minin. 2015. Vimentin is involved in regulation of mitochondrial motility and membrane potential by Rac1. *Biol. Open*. 4:1290–1297. doi:10.1242/bio.011874.

Mayerson, P.L., and J.A. Brumbaugh. 1981. Lavender, a chick melanocyte mutant with defective melanosome translocation: a possible role for 10 nm filaments and microfilaments but not microtubules. *J. Cell Sci.* 51:25–51.

Michael, D.J., R.A. Ritzel, L. Haataja, and R.H. Chow. 2006. Pancreatic β-Cells Secrete Insulin in Fast- and Slow-Release Forms. *Diabetes*. 55:600–607. doi:10.2337/diabetes.55.03.06.db05-1054.

Michael, D.J., W. Xiong, X. Geng, P. Drain, and R.H. Chow. 2007. Human Insulin Vesicle Dynamics During Pulsatile Secretion. *Diabetes*. 56:1277–1288. doi:10.2337/db06-0367.

Mishra, P., and D.C. Chan. 2016. Metabolic regulation of mitochondrial dynamics. *J Cell Biol*. 212:379–387. doi:10.1083/jcb.201511036.

Miyazaki, J., K. Araki, E. Yamato, H. Ikegami, T. Asano, Y. Shibasaki, Y. Oka, and K. Yamamura. 1990. Establishment of a pancreatic beta cell line that retains glucose-inducible insulin secretion: special reference to expression of glucose transporter isoforms. *Endocrinology*. 127:126–132. doi:10.1210/endo-127-1-126.

Moll, R., M. Divo, and L. Langbein. 2008. The human keratins: biology and pathology. *Histochem. Cell Biol.* 129:705–733. doi:10.1007/s00418-008-0435-6.

Moll, R., W.W. Franke, D.L. Schiller, B. Geiger, and R. Krepler. 1982. The catalog of human cytokeratins: Patterns of expression in normal epithelia, tumors and cultured cells. *Cell*. 31:11–24. doi:10.1016/0092-8674(82)90400-7.

Mukaka, M. 2012. A guide to appropriate use of Correlation coefficient in medical research. *Malawi Med. J. J. Med. Assoc. Malawi*. 24:69–71.

Nekrasova, O.E., M.G. Mendez, I.S. Chernoivanenko, P.A. Tyurin-Kuzmin, E.R. Kuczmarski, V.I. Gelfand, R.D. Goldman, and A.A. Minin. 2011. Vimentin intermediate filaments modulate the motility of mitochondria. *Mol. Biol. Cell*. 22:2282–2289. doi:10.1091/mbc.E10-09-0766.

Neupert, W., and J.M. Herrmann. 2007. Translocation of proteins into mitochondria. *Annu. Rev. Biochem.* 76:723–749. doi:10.1146/annurev.biochem.76.052705.163409.

Nikitakis, N.G., K.I. Tosios, V.S. Papanikolaou, H. Rivera, S.I. Papanicolaou, and O.B. Ioffe. 2004. Immunohistochemical expression of cytokeratins 7 and 20 in malignant salivary gland tumors. *Mod. Pathol. Off. J. U. S. Can. Acad. Pathol. Inc*. 17:407–415. doi:10.1038/modpathol.3800064.

Nishi, M., T. Sanke, S. Nagamatsu, G.I. Bell, and D.F. Steiner. 1990. Islet amyloid polypeptide. A new beta cell secretory product related to islet amyloid deposits. *J. Biol. Chem.* 265:4173–4176.

Nishizawa, M., I. Izawa, A. Inoko, Y. Hayashi, K. Nagata, T. Yokoyama, J. Usukura, and M. Inagaki. 2005. Identification of trichoplein, a novel keratin filament-binding protein. *J Cell Sci*. 118:1081–1090. doi:10.1242/jcs.01667.

Nussey, S., and S. Whitehead. 2001. The endocrine pancreas. BIOS Scientific Publishers.

Olympus. 2017. 2. Resolving Power of Laser Scanning Microscopes | Olympus IMS.

Omary, M.B. 2009. “IF-pathies”: a broad spectrum of intermediate filament-associated diseases. *J. Clin. Invest.* 119:1756–1762. doi:10.1172/JCI39894.

Omary, M.B., N.-O. Ku, P. Strnad, and S. Hanada. 2009. Toward unraveling the complexity of simple epithelial keratins in human disease. *J. Clin. Invest.* 119:1794–1805. doi:10.1172/JCI37762.

Omary, M.B., N.-O. Ku, and D.M. Toivola. 2002. Keratins: guardians of the liver. *Hepatol. Baltim. Md*. 35:251–257. doi:10.1053/jhep.2002.31165.

Owens, D.W., N.J. Wilson, A.J.M. Hill, E.L. Rugg, R.M. Porter, A.M. Hutcheson, R.A. Quinlan, D. van Heel, M. Parkes, D.P. Jewell, S.S. Campbell, S. Ghosh, J. Satsangi, and E.B. Lane. 2004. Human keratin 8 mutations that disturb filament assembly observed in inflammatory bowel disease patients. *J. Cell Sci.* 117:1989–1999. doi:10.1242/jcs.01043.

Pandol, S.J. 2010. Digestive Enzymes. Morgan & Claypool Life Sciences.

Park, M.K., M.C. Ashby, G. Erdemli, O.H. Petersen, and A.V. Tepikin. 2001. Perinuclear, perigranular and sub-plasmalemmal mitochondria have distinct functions in the regulation of cellular calcium transport. *EMBO J.* 20:1863–1874. doi:10.1093/emboj/20.8.1863.

Patzelt, C., A.D. Labrecque, J.R. Duguid, R.J. Carroll, P.S. Keim, R.L. Heinrikson, and D.F. Steiner. 1978. Detection and kinetic behavior of preproinsulin in pancreatic islets. *Proc. Natl. Acad. Sci. U. S. A.* 75:1260–1264.

Pekny, M., and E.B. Lane. 2007. Intermediate filaments and stress. *Exp. Cell Res.* 313:2244–2254. doi:10.1016/j.yexcr.2007.04.023.

Pfanner, N., E.A. Craig, and A. Hönlinger. 1997. MITOCHONDRIAL PREPROTEIN TRANSLOCASE. *Annu. Rev. Cell Dev. Biol.* 13:25–51. doi:10.1146/annurev.cellbio.13.1.25.

Poitout, V., D. Hagman, R. Stein, I. Artner, R.P. Robertson, and J.S. Harmon. 2006. Regulation of the insulin gene by glucose and fatty acids. *J. Nutr.* 136:873–876.

Porter, R.M., and E.B. Lane. 2003. Phenotypes, genotypes and their contribution to understanding keratin function. *Trends Genet. TIG*. 19:278–285.

Potter, H., and R. Heller. 2003. Transfection by Electroporation. *Curr. Protoc. Mol. Biol. Ed. Frederick M Ausubel Al*. CHAPTER:Unit-9.3. doi:10.1002/0471142727.mb0903s62.

Rahier, J., J. Wallon, and J.C. Henquin. 1981. Cell populations in the endocrine pancreas of human neonates and infants. *Diabetologia*. 20:540–546.

Reichert, M., and A.K. Rustgi. 2011. Pancreatic ductal cells in development, regeneration, and neoplasia. *J. Clin. Invest.* 121:4572–4578. doi:10.1172/JCI57131.

Robert, A., C. Hookway, and V.I. Gelfand. 2016. Intermediate filament dynamics: What we can see now and why it matters. *BioEssays News Rev. Mol. Cell. Dev. Biol.* 38:232–243. doi:10.1002/bies.201500142.

Robertson, P.W., and V. Kertesz. 1975. Modified Fluorescent Antibody Technique to Detect Immunoglobulin M Antibodies to Toxoplasma gondii in Congenital Infection. *J. Clin. Microbiol.* 2:461–462.

Robin, E.D., and R. Wong. 1988. Mitochondrial DNA molecules and virtual number of mitochondria per cell in mammalian cells. *J. Cell. Physiol.* 136:507–513. doi:10.1002/jcp.1041360316.

Rossignol, R., R. Gilkerson, R. Aggeler, K. Yamagata, S.J. Remington, and R.A. Capaldi. 2004. Energy substrate modulates mitochondrial structure and oxidative capacity in cancer cells. *Cancer Res.* 64:985–993.

Saito, K., N. Iwama, and T. Takahashi. 1978. Morphometrical analysis on topographical difference in size distribution, number and volume of islets in the human pancreas. *Tohoku J. Exp. Med.* 124:177–186.

Saladin, K. 2018. What is the process whereby insulin is produced in a normal human cell?

Sarria, A.J., J.G. Lieber, S.K. Nordeen, and R.M. Evans. 1994. The presence or absence of a vimentin-type intermediate filament network affects the shape of the nucleus in human SW-13 cells. *J. Cell Sci.* 107 (Pt 6):1593–1607.

Schwarz, N., and R.E. Leube. 2016. Intermediate Filaments as Organizers of Cellular Space: How They Affect Mitochondrial Structure and Function. *Cells*. 5. doi:10.3390/cells5030030.

Schweizer, J., P.E. Bowden, P.A. Coulombe, L. Langbein, E.B. Lane, T.M. Magin, L. Maltais, M.B. Omary, D.A.D. Parry, M.A. Rogers, and M.W. Wright. 2006. New consensus nomenclature for mammalian keratins. *J. Cell Biol.* 174:169–174. doi:10.1083/jcb.200603161.

Shaw, J.M., and J. Nunnari. 2002. Mitochondrial dynamics and division in budding yeast. *Trends Cell Biol.* 12:178–184.

Silvander, J.S.G., S.M. Kvarnström, A. Kumari-Ilieva, A. Shrestha, C.M. Alam, and D.M. Toivola. 2017. Keratins regulate β-cell mitochondrial morphology, motility, and homeostasis. *FASEB J. Off. Publ. Fed. Am. Soc. Exp. Biol.* 31:4578–4587. doi:10.1096/fj.201700095R.

Skelin, M., M. Rupnik, and A. Cencic. 2010. Pancreatic beta cell lines and their applications in diabetes mellitus research. *ALTEX*. 27:105–113.

Smith, T.A., P.M. Steinert, and D.A.D. Parry. 2004. Modeling effects of mutations in coiled-coil structures: case study using epidermolysis bullosa simplex mutations in segment 1a of K5/K14 intermediate filaments. *Proteins*. 55:1043–1052. doi:10.1002/prot.20089.

Steinert, P.M. 1975. The extraction and characterization of bovine epidermal alpha-keratin. *Biochem. J.* 149:39–48.

Steinert, P.M. 2001. Keratins: Dynamic, flexible structural proteins of epithelial cells. *Curr. Probl. Dermatol.* 3:193–198. doi:10.1016/S1040-0486(01)70013-0.

Steinert, P.M., D.A. Parry, E.L. Racoosin, W.W. Idler, A.C. Steven, B.L. Trus, and D.R. Roop. 1984. The complete cDNA and deduced amino acid sequence of a type II mouse epidermal keratin of 60,000 Da: analysis of sequence differences between type I and type II keratins. *Proc. Natl. Acad. Sci. U. S. A.* 81:5709–5713.

Steinert, P.M., M.L. Wantz, and W.W. Idler. 1982. O-phosphoserine content of intermediate filament subunits. *Biochemistry*. 21:177–183.

Strnad, P., T.C. Lienau, G.-Z. Tao, L.C. Lazzeroni, F. Stickel, D. Schuppan, and M.B. Omary. 2006. Keratin variants associate with progression of fibrosis during chronic hepatitis C infection. *Hepatol. Baltim. Md*. 43:1354–1363. doi:10.1002/hep.21211.

Strnad, P., Q. Zhou, S. Hanada, L.C. Lazzeroni, B.H. Zhong, P. So, T.J. Davern, W.M. Lee, Acute Liver Failure Study Group, and M.B. Omary. 2010. Keratin variants predispose to acute liver failure and adverse outcome: race and ethnic associations. *Gastroenterology*. 139:828–835, 835.e1–3. doi:10.1053/j.gastro.2010.06.007.

Styers, M.L., G. Salazar, R. Love, A.A. Peden, A.P. Kowalczyk, and V. Faundez. 2004. The Endo-Lysosomal Sorting Machinery Interacts with the Intermediate Filament Cytoskeleton. *Mol. Biol. Cell*. 15:5369–5382. doi:10.1091/mbc.E04-03-0272.

Summerhayes, I.C., D. Wong, and L.B. Chen. 1983. Effect of microtubules and intermediate filaments on mitochondrial distribution. *J. Cell Sci.* 61:87–105.

Szeverenyi, I., A.J. Cassidy, C.W. Chung, B.T.K. Lee, J.E.A. Common, S.C. Ogg, H. Chen, S.Y. Sim, W.L.P. Goh, K.W. Ng, J.A. Simpson, L.L. Chee, G.H. Eng, B. Li, D.P. Lunny, D. Chuon, A. Venkatesh,

K.H. Khoo, W.H.I. McLean, Y.P. Lim, and E.B. Lane. 2008. The Human Intermediate Filament Database: comprehensive information on a gene family involved in many human diseases. *Hum. Mutat.* 29:351–360. doi:10.1002/humu.20652.

T Sun, T., R. Eichner, W. G. Nelson, S. Tseng, R. Weiss, M. Jarvinen, and J. Woodcock-Mitchell. 1983. Keratin Classes: Molecular Markers for Different Types of Epithelial Differentiation. 81. 109s pp.

Tanaka, Y., Y. Kanai, Y. Okada, S. Nonaka, S. Takeda, A. Harada, and N. Hirokawa. 1998. Targeted Disruption of Mouse Conventional Kinesin Heavy Chain kif5B, Results in Abnormal Perinuclear Clustering of Mitochondria. *Cell*. 93:1147–1158. doi:10.1016/S0092-8674(00)81459-2.

Tao, G.-Z., K.S. Looi, D.M. Toivola, P. Strnad, Q. Zhou, J. Liao, Y. Wei, A. Habtezion, and M.B. Omary. 2009. Keratins modulate the shape and function of hepatocyte mitochondria: a mechanism for protection from apoptosis. *J. Cell Sci.* 122:3851–3855. doi:10.1242/jcs.051862.

Toivola, D.M., P. Boor, C. Alam, and P. Strnad. 2015. Keratins in health and disease. *Curr. Opin. Cell Biol.* 32:73–81. doi:10.1016/j.ceb.2014.12.008.

Toivola, D.M., S. Krishnan, H.J. Binder, S.K. Singh, and M.B. Omary. 2004. Keratins modulate colonocyte electrolyte transport via protein mistargeting. *J. Cell Biol.* 164:911–921. doi:10.1083/jcb.200308103.

Toivola, D.M., G.-Z. Tao, A. Habtezion, J. Liao, and M.B. Omary. 2005. Cellular integrity plus: organelle-related and protein-targeting functions of intermediate filaments. *Trends Cell Biol.* 15:608–617. doi:10.1016/j.tcb.2005.09.004.

Veatch, J.R., M.A. McMurray, Z.W. Nelson, and D.E. Gottschling. 2009. Mitochondrial dysfunction leads to nuclear genome instability via an iron-sulfur cluster defect. *Cell*. 137:1247–1258. doi:10.1016/j.cell.2009.04.014.

Veltri, K.L., M. Espiritu, and G. Singh. 1990. Distinct genomic copy number in mitochondria of different mammalian organs. *J. Cell. Physiol.* 143:160–164. doi:10.1002/jcp.1041430122.

Verschoor, A., and T. Lithgow. 1999. A First Glimpse at the Structure of the Tom Translocase from the Mitochondrial Outer Membrane. *J. Cell Biol.* 147:905–908.

Weiss, M., D.F. Steiner, and L.H. Philipson. 2000. Insulin Biosynthesis, Secretion, Structure, and Structure-Activity Relationships. *In* Endotext. L.J. De Groot, G. Chrousos, K. Dungan, K.R. Feingold, A. Grossman, J.M. Hershman, C. Koch, M. Korbonits, R. McLachlan, M. New, J. Purnell, R. Rebar, F. Singer, and A. Vinik, editors. MDText.com, Inc., South Dartmouth (MA).

Weiss, M.A. 2009. Proinsulin and the Genetics of Diabetes Mellitus. *J. Biol. Chem.* 284:19159–19163. doi:10.1074/jbc.R109.009936.

Welsh, M., D.A. Nielsen, A.J. MacKrell, and D.F. Steiner. 1985. Control of insulin gene expression in pancreatic beta-cells and in an insulin-producing cell line, RIN-5F cells. II. Regulation of insulin mRNA stability. *J. Biol. Chem.* 260:13590–13594.

Whitcomb, D.C., and M.E. Lowe. 2007. Human pancreatic digestive enzymes. *Dig. Dis. Sci.* 52:1–17. doi:10.1007/s10620-006-9589-z.

Wickstead, B., and K. Gull. 2011. The evolution of the cytoskeleton. *J. Cell Biol.* 194:513–525. doi:10.1083/jcb.201102065.

Wilson, A.K., P.A. Coulombe, and E. Fuchs. 1992. The roles of K5 and K14 head, tail, and R/K L L E G E domains in keratin filament assembly in vitro. *J. Cell Biol.* 119:401–414.

Wilson, N., E. O'Toole, L. Milstone, C. Hansen, A. Shepherd, E. Al-Asadi, M. Schwartz, W. McLean, E. Sprecher, and F. Smith. 2014. The molecular genetic analysis of the expanding pachyonychia congenita case collection. *Br. J. Dermatol.* 171:343–355. doi:10.1111/bjd.12958.

Winter, L., C. Abrahamsberg, and G. Wiche. 2008. Plectin isoform 1b mediates mitochondrion-intermediate filament network linkage and controls organelle shape. *J. Cell Biol.* 181:903–911. doi:10.1083/jcb.200710151.

Yano, M., K. Terada, and M. Mori. 2003. AIP is a mitochondrial import mediator that binds to both import receptor Tom20 and preproteins. *J. Cell Biol.* 163:45–56. doi:10.1083/jcb.200305051.

Yi, M., D. Weaver, and G. Hajnóczky. 2004. Control of mitochondrial motility and distribution by the calcium signal: a homeostatic circuit. *J. Cell Biol.* 167:661–672. doi:10.1083/jcb.200406038.

Züchner, S., I.V. Mersiyanova, M. Muglia, N. Bissar-Tadmouri, J. Rochelle, E.L. Dadali, M. Zappia, E. Nelis, A. Patitucci, J. Senderek, Y. Parman, O. Evgrafov, P.D. Jonghe, Y. Takahashi, S. Tsuji, M.A. Pericak-Vance, A. Quattrone, E. Battaloglu, A.V. Polyakov, V. Timmerman, J.M. Schröder, J.M. Vance, and E. Battologlu. 2004. Mutations in the mitochondrial GTPase mitofusin 2 cause Charcot-Marie-Tooth neuropathy type 2A. *Nat. Genet.* 36:449–451. doi:10.1038/ng1341.